NASA Technical Paper 3052

October 1990

Flow-Induced Resonance of Screen-Covered Cavities

Paul T. Soderman

NASA

NASA Technical Paper 3052

1990

Flow-Induced Resonance of Screen-Covered Cavities

Paul T. Soderman
Ames Research Center
Moffett Field, California

National Aeronautics and Space Administration
Office of Management
Scientific and Technical Information Division

SYMBOLS

c	sound speed, m/sec
d	perforation hole diameter, mm
f_c	cavity modal frequency, Hz
f_v	predicted vortex shedding frequency of orifice, Hz
ℓ	streamwise center to center hole spacing of perforation, mm
Lp	sound pressure level, dB relative to 2×10^{-5} N/m^2
L_x	cavity depth in cross-stream direction, mm
L_y	cavity width in streamwise direction, mm
L_z	cavity height, mm
M	Mach number
n	integer number of vortex spacings or wavelengths between two hot wires
n_x	room mode in depth or cross-stream direction of cavity
n_y	room mode in width or streamwise direction of cavity
n_z	room mode in vertical direction of cavity
p(t)	acoustic pressure as a function of time, N/m^2
p_{rms}	root mean square of acoustic pressure, N/m^2
q	test section dynamic pressure measured upstream of the vanes, N/m^2
St	Strouhal number
u'	unsteady streamwise velocity component (rms), m/sec
U	local time average wind speed, m/sec
U_o	average wind speed at duct cross section containing vane(s), m/sec
U_c	average convection speed of periodic flow structure in boundary layer, m/sec
x	distance downstream from leading edge of cavity, mm
x_w	streamwise distance between two hot wires, mm
y	perpendicular distance from screen; positive into cavity interior, mm
z	distance down from top edge of cavity, mm

δ	boundary-layer depth, mm
Δ Lp	uncalibrated sound level, dB
Δ Lv	20 times log to base 10 of rms voltage, dB
$\Delta\tau$	delay time for propagation of vortex from one hot wire to another, sec
$\Delta\tau_o$	delay time to first cross-correlation peak in hot wire signals, sec
$\Delta\tau_1$	delay time or period of one vortex wavelength in the cross correlation, sec
λ_v	wavelength of periodic flow structure in boundary layer; equal to vortex spacing, mm

SUMMARY

This report describes an experimental study of screen-covered cavities exposed to airflow tangent to the screen. In this study, the term "screen" refers to a thin metal plate perforated with a repetitive pattern of round holes. Cavities are a necessary feature of many fluid systems, but the associated pressure fluctuations in cavities, both aerodynamic and acoustic, are often highly undesirable. In many cases, screen coverings are compatible with the intended communication between the cavity and airstream, but their interaction with the free stream can induce cavity acoustic resonance. The purpose of this investigation was to find the detailed aerodynamic and acoustic mechanisms responsible for screen-covered cavity resonance and to find ways to control the pressure oscillations.

Results of the study indicate that strong cavity acoustic resonances are created by screen orifices that shed vortices which couple with cavity pressure oscillations. The screen geometry plays a dominant role in the resonance. A method was found to avoid cavity resonance by choosing hole spacings such that shed vortices do not arrive at a downstream orifice in synchronization with cavity pressure oscillations. The proper hole pattern is effective at all airspeeds. It was also discovered that a reduction of orifice size tended to weaken the screen/cavity interaction regardless of hole pattern, probably because of viscous flow losses at the orifices.

The screened cavities that resonated did so at much higher frequencies than the equivalent open cavity. The classical large eddy rotation in the open cavity is replaced by a cavity acoustic resonance, which is triggered by orifice vortex shedding. Since that phenomenon occurs at the relatively small scale of the orifices, the excitation is typically of high frequency.

The wind tunnel study was made at airspeeds from 0 to 100 m/sec. The 457-mm-long by 1.09-m-high rectangular cavities had length-to-depth ratios greater than one, which is indicative of shallow cavities. The cavity screens were perforated in straight rows and columns with hole diameters ranging from 1.59 to 6.35 mm and with porosities from 2.6 to 19.6%.

INTRODUCTION

The subject of this paper is flow-induced resonance in cavities. This problem came to our attention during the development of resonant cavity acoustic baffles for wind tunnels. Under certain conditions, the baffle resonance became uncontrolled and strong cavity oscillations were generated. Actually, there are many situations where aerodynamic or acoustic communication between a cavity and adjacent airstream is required. In most cases, gross flow pertubations in open cavities induced by the external flow are not desired. Numerous studies of cavities with single openings have been made to identify the aeroacoustic mechanisms involved and to devise methods for defeating the oscillations. Many of these methods involve modifications to the edges of the opening which alter the cavity fluctuations . For example, Heller and Bliss (1975) used spoilers and ramps on the downstream edge of open cavities to reduce cavity pressure oscillations. However, large scale eddies in open cavities cannot be eliminated entirely.

One approach to the problem is to avoid the open cavity altogether by covering it with a screen. In this report, the term "screen" will refer to a thin metal plate perforated with a repetitive pattern of round holes. Such partially covered cavities could be used to house heat exchangers, aircraft weapon stores, acoustic sensors, sound absorbers, chemical analysis equipment, or other devices. Since the screen is the interface between the cavity and the airflow, it should be possible to minimize the cavity acoustic and aerodynamic oscillations by the judicious design of the perforation pattern. Indeed, the present study indicates that screens can be used to control cavity pressure fluctuations.

A number of studies of the singing of perforated duct linings have been reported. Tsui and Flandro (1977) identified the vortex shedding over perforates as the primary mechanism for cavity resonance excitation. However, they studied a limited number of perforation geometries and did not uncover the importance of hole spacing on the aeroacoustic coupling. Bauer and Chapkis (1976) documented noise levels as high as 158 dB at the surface of a duct liner, but made no aerodynamic measurements. Dougherty et al. (1976) studied edge tones in perforated wind tunnel walls and showed that splitter plates and other geometric modifications to the orifices could suppress the edge tones.

This report describes an experimental study of flow-induced resonances in screened rectangular cavities, which were installed in the sides of simple flat-sided airfoils mounted in the NASA Ames 7- by 10-Foot Wind Tunnel. This geometry had been used in a previous investigation in the same facility of resonant-cavity duct baffles designed to attenuate sound (Soderman, 1981 and 1982). In that study, screens on baffles were used to protect internal cavities from large-scale flow pertubations and, through viscous flow interactions at the perforations, absorb sound by the transformation of acoustic energy

into heat. However, it was found that cavities covered by perforated screens could resonate and generate loud tones depending on flow conditions. Although certain screens seemed to suppress the resonance, it was decided to line the cavity internal surfaces with sound absorbent material and thereby eliminate the tones. The present study was initiated to determine the true role of cover screens in the cavity resonance phenomenon. It would then be possible to deal with situations where screens would be desirable to protect unlined cavities exposed to airflow. It is often impractical to line the cavities with sound absorbent material to suppress tones.

FACILITY, APPARATUS, AND INSTRUMENTATION

The experiment was conducted in the Ames 7- by 10-Foot Wind Tunnel No. 1 using the following apparatus and instrumentation for generating cavity resonances and measuring the aerodynamic and acoustic fields.

Wind Tunnel

The NASA Ames 7- by 10-Foot Wind Tunnel No. 1 is a closed-circuit wind tunnel with a closed test section as shown in figure 1. Acoustic treatment in the end legs of the circuit attenuates fan noise (Soderman and Hoglund, 1979). Nonetheless, drive-fan tones are visible in spectral data recorded in the test section. The blade-passage frequency of the eight-bladed fan, which was a maximum of 32 Hz at 100 m/sec airspeed, was much lower than the frequency of the acoustic data of interest. Although the test section can be used with sound absorbent walls or with three sides removed, the present study was conducted with the hard wall configuration.

Vanes and Cavities

Two simple sheet metal vanes were used to house the rectangular cavities investigated in this study. One of the two vanes is shown in figure 2 mounted floor to ceiling in the test section. In this photo, the right vane, looking upstream, has been removed. The vane geometries are given in figures 3(a) - (c). The vanes had 1.22-m chords of 305 mm thickness and were separated from each other by a 616-mm gap. Each vane had a semicircular nose, flat sides, and a boattail.

The basic cavity in each vane shown schematically in figure 4 was 302 mm deep, 457 mm long streamwise, and 1.09 m high. Cavity depth could be changed to 152 mm. Hence, the length-to-depth ratio varied from 1.5 to 3.0. Length-to-depth ratios greater than one are characteristic of shallow cavities. The two cavities, one in each vane, faced each other so that acoustical interactions could be evaluated. During parts of the study, either or both cavities were closed by a steel plate. The classical open (unscreened) cavity was also evaluated. Finally, the right vane (looking upstream) was removed and measurements were made of single vane, single cavity resonance.

To define probe locations, a coordinate system (x, y, z) is used where x is the distance downstream from the cavity leading edge, y is the perpendicular distance from the screen (positive to the interior of the cavity), and z is the cross stream distance along the screen from the cavity edge (down from the top of the cavity in this experiment).

Screens

The cavity cover screens were flush with the vane sidewall. The screens were formed from 0.91-mm-thick steel sheets perforated with holes punched on straight rows and columns as shown in figure 5(a). Eight screens were separately evaluated with perforated hole patterns listed in table 1. The hole diameter ranged from 1.59 to 6.35 mm and the hole spacing varied from 4.37 to 12.7 mm. The screen porosity ranged from 2.6% to 19.6%. Figure 5(b) is a photograph of screen no. 1 mounted on the left vane.

Microphones

Three microphones were used to record the cavity tones: one upstream (no. 1), one downstream (no. 2), and one in the cavity (no. 3) as illustrated in figures 3(a) - (c). The B&K 4133 13 mm—(one-half-inch)—diameter condenser microphone with a cone-shaped nose is robust and has a nearly uniform frequency response between 6 Hz and 15 kHz. The nose cone makes the microphone reasonably omnidirectional. The two microphones in the airstream were pointed upstream to minimize flow noise.

Figure 6 shows the struts used to support microphones no. 1 and no. 2. The strut tubing had a fairly blunt trailing edge. Because of potential vortex shedding (Soderman 1976), a boundary-layer trip was created by attaching duct tape to each strut leading edge with the sticky side out. The tape covered the strut nose from 20% chord to 20% chord. The tape viscosity and surface discontinuity created a turbulent boundary layer and eliminated coherent vortex shedding and strut tones.

The cavity microphone no. 3 illustrated in figure 3(c) was attached to the end of a 15.9-mm-diameter tube and inserted through a hole in the top of the cavity. The tube made a tight fit in the hole and was marked so that microphone depth could be measured as the tube was slid up

and down. By pivoting the tube at the hole in the cavity, the microphone could be moved in a calibrated arc to measure acoustic pressure variations in the depth direction or in the streamwise direction. The slots in the test section ceiling which allowed tube movement (fig. 3(c)) did not communicate with the airstream. Because the cavity acoustic pressures varied little in the vertical direction, the measurements along the arcs were equivalent to measurements along a line perpendicular to or parallel to the cover screen.

Acoustic Instrumentation and Data Reduction

Figure 7 shows the acoustic data acquisition and reduction equipment. A narrow-band spectrum analyzer was used to digitize and plot the frequency domain data as well as store the spectra on disc files. The data were later transferred to a computer, adjusted for amplifier gain, and cross plotted. The data were also recorded on an analog tape recorder for backup. The narrow-band spectra had a 10-kHz or 20-kHz maximum frequency range, which resulted in constant bandwidths of 12.5 Hz and 25 Hz, respectively. A Hanning window minimized leakage during the Fast Fourier Transform (FFT) process.

Aerodynamic Instrumentation and Data Reduction

Test-section dynamic pressure, q, was measured with a floor mounted pitot-static probe 1.58 m upstream of the vanes as shown in the lower right corner of figure 2. Barometric pressure and test-section temperature were used to find the air density. The density and dynamic pressure data were then used to compute airspeed. Because one vane blocked 10% of the duct cross section and two vanes blocked 20% of the cross section, the flow accelerated from the probe location to the vane location. Assuming incompressible flow, the velocity at the pitot-static probe was corrected to the average velocity at the vanes by multiplying the airspeed at the probe by the area ratios of the two flow cross sections, namely 1.11 or 1.25, depending on whether one or two vanes were installed, respectively.

Dynamic pressures were also measured near the vanes with a traversing pitot-static probe shown in figure 8. This traverse assembly also supported a single hot wire that was used to measure turbulent and mean velocities. The probe assembly was mounted to a tube cantilevered from a horizontal survey strut downstream of the vanes. The horizontal survey strut was 1.09 m downstream from the pitot-static probe tip. The hot wire was oriented vertically so that it could be placed very close to the screen in order to measure streamwise velocities. The hot-wire and pressure signal processing equipment is shown in figure 9. The hot-wire anemometer output voltage was not linearized. Air velocity was deduced from the nonlinear response by employing a calibration scheme described in the Appendix. Turbulent velocities, mean velocities, and turbulence spectra were acquired. This hot wire was used to measure boundary-layer profiles and disturbances in the boundary layer near the holes.

A fixed hot wire was mounted to a strut adjacent to the left vane as shown in the lower part of figure 8. With the fixed single wire located adjacent to a hole in the screen, for example, the traversing hot wire could be moved downstream from the wire to record signal correlations and convection speeds. During most boundary-layer surveys, the traversing hot wire was positioned far from the fixed hot wire in order to avoid flow interactions.

During selected runs, the cavity temperature was monitored using a thermocouple. The wind tunnel temperature measured on the settling chamber turning vanes was usually 1° C cooler than the cavity temperature and thus could be relied on for estimating cavity temperatures. Barometric pressure and relative humidity were also recorded.

EXPERIMENTAL METHOD

Wind-tunnel speed was varied from 0 to 100 m/s. The maximum chord based Reynolds number of the vanes was 8.4 19 ¥ 10^6. Flow surveys or time-averaged acoustic data were acquired while airspeed was held constant. In some cases, the airspeed was chosen to correspond to the initial occurrence of a particular cavity tone as determined by ear. The tones were usually quite distinct and, in some cases, were strong enough to annoy people in an adjacent building.

Wind tunnel background noise and flow noise were documented by recording sound level versus airspeed with the cavities sealed by 0.9-mm thick steel plates. This was repeated for single and double vane operation. In some cases, tones from the wind tunnel were as strong as the weaker tones generated by the cavity. However, the background noise spectra made it possible to identify most cavity and non-cavity tones. The predicted fundamental vibrational frequency (structural) of the cavity cover plates and screens was 13 Hz, far below the cavity aeroacoustic resonance frequencies.

The primary purpose of gathering the acoustic data was to confirm the occurrence of cavity resonance, the frequency of the resonance tones, and the relative changes in the tone strength with airspeed and/or model geometry. Because the test-section walls were untreated, the acoustic

levels at the upstream or downstream microphones no. 1 and no. 2 were contaminated by reflections. However, free-field tone levels were not required and the frequencies of the tones were consistently recorded by all three microphones. The change in the amplitude of the tones as the flow condition or cavity geometry was varied could be readily followed by all three microphones. The cavity microphone no. 3 was the least affected by reflections in the test section.

Hot-wire surveys of the vane boundary layer were made with a computer-controlled survey system. The wire position was measured before and after each run, and it was found that, though there was no direct readout of wire position, the digital stepper motors faithfully followed the computer commands. It is estimated that the wire position was accurate to ±0.7 mm. The hot-wire voltage and computed velocity were calibrated against the traverse pitot-static data with the probes positioned in the free stream where steady, streamwise velocities were assured.

An attempt was made to visualize the periodic flow in and out of the perforations during cavity resonance by allowing smoke to filter out of the holes while an external strobe lamp lit the vane at a rate equal to the resonance frequency. However, the airspeed required for resonance was sufficiently high to blow the smoke away before a periodic flow could be seen. The smoke did show, however, that the flow over the leading edge of the screen was separated. The flow reattached to the screen around 100 mm downstream from the screen leading edge. In that first 100 mm, the flow over the screen appeared to be chaotic, though there was evidence of a trapped vortex or recirculation in the separation bubble. Downstream of the reattachment line, the smoke showed that the flow was streamwise and much smoother. Thus, our boundary-layer measurements were done considerably downstream of the flow reattachment. The flow separation was probably caused by air pumping out of the screened cavity just downstream of the semicircular nose. The shape of the nose must have induced high velocities and low surface pressures in that region that were lower than the cavity pressure. Cavity inflow probably occurred near the tail. A nose shaped more like an airfoil might have eliminated the flow separation. In any case, the flow separation had no effect on the aeroacoustic study.

RESULTS AND DISCUSSION

Feedback Loop Mechanism

Cavity resonance is driven by a feedback loop mechanism which involves several acoustic and aerodynamic parameters. To understand the relationship of the various experimental parameters to be discussed, it helps to keep in mind the feedback loop sequence. As will be shown, the data obtained in this experiment are consistent with the following model for resonance of the rectangular cavity covered by a perforated plate.

1. As the airspeed over the vane is increased from zero, a speed is reached where the unsteady shear layer oscillations in each orifice allow the free-stream air to enter the cavity periodically and thereby generate cavity pressure fluctuations. The pumping action at the orifices creates a periodic flow structure in the boundary layer which moves downstream and interacts with the next hole.

2. The cavity pressure fluctuations excite cavity acoustic pressure resonance at a cavity "room" mode having a frequency near the frequency of the flow oscillation. Usually, other weaker cavity modes are also excited that are most likely adjacent modes or harmonics of the dominant mode. The acoustic pressures radiate to the far field as tones.

3. The cavity acoustic pressures interact with the orifice oscillations in such a way as to amplify those oscillations and lock the frequencies of the oscillations to the cavity modes. In turn the orifice oscillations transfer free-stream energy into the cavity and energize the cavity acoustic mode.

4. As airspeed is increased further, the orifice pumping rate will increase and acoustic energy in the dominant cavity mode will decrease, while the energy in the higher mode(s) increases. The orifice pumping rate always matches an acoustic modal frequency.

If a cavity and screen has the proper geometry for resonance (as will be explained) and the flow speed is above the minimum required, the resonant condition is very stable. However, resonance can be avoided by breaking the feedback loop. For example, previous studies (Soderman, 1981 and 1982) showed that sound absorbent material in the cavity eliminates resonance at all airspeeds. Alternatively, breaking the aerodynamic/ acoustic coupling at the screen will also block resonance, which was the method sought in this study.

The resonance depends on how the holes interact with each other. As will be shown, the periodic flow emitted from each orifice must arrive at the next downstream orifice with the proper phase if resonance is to be sustained. The frequency and phase of the periodic flow are controlled by the oscillation or shedding rate, convection speed, hole spacing, and cavity resonance frequency.

Oscillatory Flow on the Screen

Hot-wire measurements confirmed that, during cavity resonance, there was a periodic flow structure in the boundary layer shown on the screen. Figure 10 illustrates the hot-wire turbulence spectrum measured during cavity resonance with the wire located 1.59 mm from screen no. 1 on the normal to a hole. A periodic velocity with an rms magnitude of 0.71 m/sec occurred at 3475 Hz. That velocity was approximately 1.6 percent of the free-stream velocity U_0. (The unfiltered rms turbulence level was 8% of the free-stream velocity at that position in the boundary layer.) The hot wire was reacting to the flow pumping in and out of the hole, though the velocity direction can not be determined from one wire. The upper curve in figure 10 is the corresponding acoustic spectrum in the cavity. Harmonics at twice and three times the dominant frequency are visible in both the microphone and hot-wire signals. This indicates that two or more periodic oscillations were superimposed in the flow over the screen.

The hot wire responds to both aerodynamic and acoustic velocity fluctuations. However, if it is assumed that the fundamental tone in figure 10 was created by the velocity in a sound wave, the computed sound level of 143 dB is 18 dB greater than the sound level in the cavity, whereas the sound should decrease from the cavity outward. Furthermore, we found that the strong hot-wire tone could only be found in the wake of an orifice. The periodic signal was not found with the hot wire located between orifice rows. Also there were no electronic tones in the hot-wire signal near the measured tone. Hence, the periodic velocity was aerodynamic in nature.

This variation of oscillatory flow with hot-wire position is illustrated in figure 11. The strong oscillatory flow is present in the wake of each orifice and extends to the next hole, but not above or below an orifice row. In the direction perpendicular to a screen orifice with 3.18 mm diameter, the periodic oscillation was visible in the hot-wire signal out to a distance of 5 mm, at which point the signal disappeared in the boundary-layer turbulence spectrum. (It is logical that the height of the disturbance depends on hole diameter.) Continuing into the smooth flow outside the boundary layer, the hot wire picked up the relatively weak periodic signal which proved to be an acoustic velocity that was measurable out to a distance of 102 mm. To summarize, the acoustic tones from the cavity propagated throughout the test section, but the aerodynamic oscillations near the screen were visible only within 5 mm of screen no. 1 and in line with a row of orifices.

In one series of experiments, we attached a 17.5-mm-high spoiler to the leading edge of the screen as shown in figure 12. According to the hot-wire signal, the chaotic flow behind the spoiler swamped the oscillatory flow in the wake of the orifices. There was, however, a weak tone still present in the cavity. The resonance with the spoiler was attenuated 32 dB relative to the tone level in the cavity when a spoiler was not present.

Orifice Vortex Shedding

Baumeister and Rice (1975) also studied the periodic wake flow of an orifice in a resonator exposed to grazing flow. Their photographs of the orifice flow during a simulated resonance cycle, which are reproduced in figure 13, show the vortex-like flow which is ejected from the orifice on the outflow. Oscillations of air in and out of an orifice create a sequence of ring vortices (visible in other photos by Baumeister and Rice, 1975) which, because of the grazing flow, quickly deform into the rotating eddies shown in the photographs. The eddies can be characterized as a row or street of vortices, all rotating in the same direction. (The screen reflection is equivalent to a row of vortices parallel to and of opposite rotation to the real ones.) Our hot-wire data suggest that a similar flow field was created on the cavity screen since the measured location and periodic nature of the disturbance is consistent with the photographs of figure 13. Note that the eddy height in figure 13 is roughly equal to the orifice diameter, which agrees with our hot-wire measurements near screen no. 1.

The natural vortex shedding rate of the vortex street on the screen is given by

$$f_v = \frac{St\ U_o}{d} \qquad (1)$$

Our data indicate that if resonance occurs, the vortex shedding rate, f_v , must correspond to a cavity modal frequency, f_c. The modal resonance locks the vortex shedding rate to a modal frequency which occurs in the spectrum near f_v. Other vortex shedding rates will also be generated corresponding to adjacent cavity modes or higher harmonics of the dominant mode. Furthermore, the shedding rate at resonance is strongly affected by the phase coupling between the vortices and cavity pressure fluctuations as will be explained.

By examining the set of tones from screens with three different hole diameters, it was found that the Strouhal number in equation 1 varied with hole diameter according the following empirical fit to the data.

$$St = m\,(-0.01 + 0.10\,d) \qquad (2)$$

where m = 1, 2, 3, ...

and the hole diameter, d, is measured in millimeters. The value m = 1 in the above Strouhal relationship corresponds to vortex shedding at the dominant resonance frequency. In several cases, weak tones were observed at multiples corresponding to m = 2 and 3. Equation 2 is comparable to the Strouhal relationship given by Tsui and Flandro (1977), who studied resonant cavity wall linings and found that the Strouhal number in their experiments varied as 0.15 + 0.02 d. For screen no. 1, which had a hole diameter of 3.18 mm, equation 2 gives a Strouhal number of 0.31, a number that could be used for the vortex shedding rate of bluff bodies. De Metz and Farabee (1977) proposed that the Strouhal number for deep cavity resonance depends on boundary-layer thickness. If the boundary-layer thickness of screen no. 1 is incorporated in their equation, the Strouhal number predicted by De Metz and Farabee is approximately 0.22.

Convection Speed and Boundary-Layer Profile

An estimate of vortex convection speed in the boundary layer is essential to understanding how the vortices interact with the holes and the cavity pressures. Two methods were used to determine vortex convection speed. 1) Signals from two hot wires, one upstream of the other, were cross correlated to find the vortex propagation time between the wires. 2) Boundary-layer velocity profiles were measured and the convection speed was deduced from the estimated height of the vortices in the boundary layer.

The vortex convection speed normalized by the free-stream velocity was found to fall in the range

$$0.5 \le \frac{U_c}{U_o} \le 0.75 \qquad (3)$$

The convection speeds of orifices that had large holes and spacings fell mainly in the upper part of the range, and the convection speeds of orifices that had small holes and small spacings were lower. This variation appears to depend on location of the vortices in the boundary layer as they move downstream. The following paragraphs describe the assumptions and computations used to arrive at the relationship given in equation 3.

The first method used to determine convection speed of the vortices as they moved along the screen involved the measurement of the cross correlation of two hot wires located near screen no. 1. Recordings were made with the wires separated by several streamwise distances. However, the results were complicated by the periodic nature of the flow and the resulting periodic correlation. Figure 14 shows the cross correlation from two hot wires spaced x_w = 15.9 mm apart and positioned 1.6 mm from the screen. Since the peak correlation was observed to occur periodically, the delay time for propagation from one wire to another, $\Delta\tau$, is ambiguous because it is not clear which pair of peaks correspond to the propagation time. However, if the number of wavelengths (or distance between vortices) that occur between the wires could be estimated, the propagation time between wires could be calculated.

Consider the following periodic vortex velocity structure in the boundary layer at one instant in time. The waves are moving from left to right with a convection speed, U_c, past two hot wires, as shown in the following sketch. The wires are spaced a distance x_w apart, which is equal to the wave convection speed times the propagation time from one wire to the next. From the cross correlation

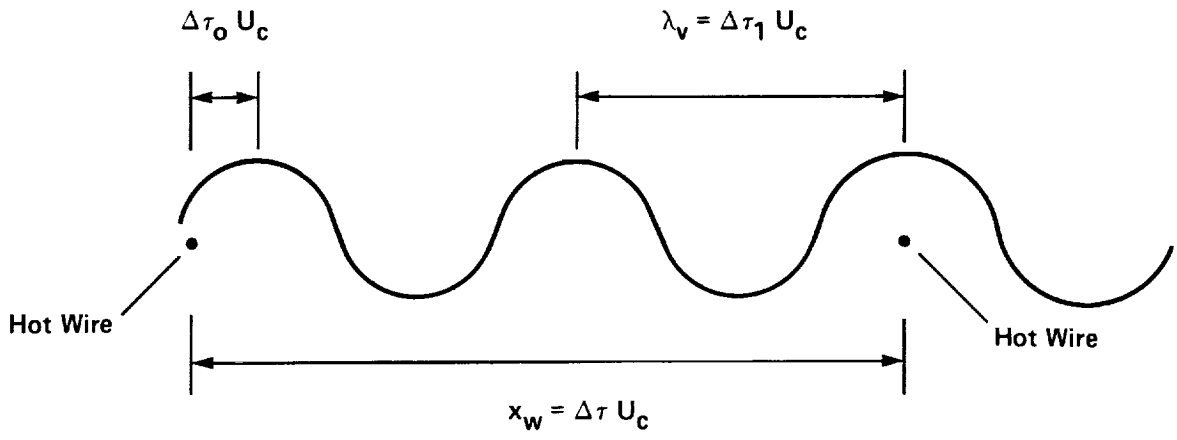

of the hot-wire signals (fig. 14), the wave period $\Delta\tau_1$ is measured. If the wires had happened to be positioned an even number of wavelengths apart, the cross correlation would show a peak at zero time and at successive times spaced $\Delta\tau_1$ apart. Since the wires were not positioned an even number of wavelengths apart, the cross correlation has a time shift $\Delta\tau_o$ to the first correlation peak, which corresponds to the phase shift between the wires illustrated in the above sketch. Finally, if the number of complete wavelengths between the wires, n, could be estimated, the convection speed could be computed from the following relationship.

$$x_w = \Delta\tau\ U_c = n\ \Delta\tau_1 U_c + \Delta\tau_o U_c \qquad (4)$$

and

$$U_c = x_w / [n\ \Delta\tau_1 + \Delta\tau_o\ ] \qquad (5)$$

To illustrate the use of equation 5, consider the cross correlation data shown in figure 14. The wire spacing was x_w = 15.9 mm. The period of one wavelength, $\Delta\tau_1$, is the inverse of the resonance frequency or 0.289 msec and the first correlation peak occurred at $\Delta\tau_o = -0.13$ msec. If we assume that slightly less than three vortex wavelengths existed between the wires, then n = 3 and the convection speed given by equation 5 is 21.6 m/s, which is 52 % of the free-stream velocity, U_O. In this analysis, the value of n was chosen to give a convection speed that was consistent with the following independent estimate of convection speed using the boundary-layer velocity profile described next. In other words, the wrong choice of n results in a ridiculous value of convection speed. Because of possible experimental inaccuracies associated with measuring very small quantities, this method results in an estimated value of relative convection speed with error band of $U_C / U_O = 0.52 \pm 0.15$.

The second method for determining convection speeds of the small-scale vortices involved measurements of the boundary-layer velocity profile and estimates of the position of the vortices in the boundary layer. Figure 15(a) shows the boundary-layer profile measured 368 mm downstream from the leading edge of screen no. 1 using a hot-wire traverse normal to the screen. The traverse was made in-line and out-of-line with a row of holes during cavity resonance. The boundary-layer depth was approximately 27 mm. Both velocity profiles have the classical shape of a turbulent boundary layer as illustrated by figure 15(b), which has a theoretical boundary-layer profile superimposed on the data. The theoretical profile (eq. 6) is a plot of the following one-seventh power law, where the height of the boundary layer, δ, was 27 mm.

$$\frac{U}{U_o} = \left(\frac{|y|}{\delta}\right)^{\frac{1}{7}} \qquad (6)$$

Note on figure 15(a) the reversal of the in-row data curve near y = –5 mm caused by the small jet of air emitting from the orifice. (The survey was made directly over a hole.) This is another example of the fluid pumping action at the orifices. Other than the velocity inflection, the two curves from data measured in-row and out-of-row have a similar shape with slightly more turbulence (i.e., lower velocities) in line with the holes as compared with out of line. Apparently, the holes create a surface roughness that impedes the airflow.

The idea that convection speed is equal to the local velocity in the boundary layer agrees with the work of Favre et al. (Schlichting, 1968) who measured convection speeds of eddies in a flat plate turbulent boundary layer using cross correlation. They found an eddy convection speed of 0.8 U_O at a distance from the wall of $|y| / \delta = 0.24$. We found that the boundary-layer velocity was also equal to 0.8 U_O at that height (fig. 15(a)). Therefore, we conclude that the small-scale eddy convection speed is equal to the boundary-layer velocity measured with a single hot wire.

Now, since the local velocity varies with the vertical location in the boundary layer, the convection speed of the small-scale vortices must also depend on the height of the vortices in the boundary layer. It is reasonable to assume that large orifices would eject air to a greater height in the boundary layer than small orifices. Since the vortices on screen no. 1 were identified in the boundary layer out to 5 mm from the screen, it is estimated that the vortex convection speed was between 0.5 and 0.75 times the free-stream velocity for screen no. 1. A value of U_C / U_O = 0.65 was chosen for that screen, which had 3.18-mm diameter holes. Analysis of the spectral data indicated that the convection speed of other hole patterns also fell in the range given by equation 3.

In reality, the average vortex convection speed is an approximation because the motion of the vortices from one hole to another may be quite complicated if analyzed in detail. As the air is pumped out of the orifices, the vortices begin to form very close to the screen where the velocity is close to zero and, as the vortices grow and rise in the boundary layer, they will accelerate according to the boundary-layer velocity gradient. Remnants of the

original ring vortex would induce the vortices even higher. Thus, the farther the vortices travel, the higher they will rise in the boundary layer and the greater will be their velocity. The effect of this on the data interpretation will be discussed in the section on the effect of hole diameter and spacing on resonance.

Cavity Modes

Like all acoustical resonators, the cavities in this study would resonate only at frequencies which corresponded to modes. Of the various types of modes possible, namely Helmholtz modes, depth modes, and room modes, a careful examination of the data showed that the screen-covered cavities invariably resonated at room modes involving the cavity depth and width. This indicates that even though the screen was porous and allowed acoustic energy to escape, the cavity pressure fluctuations acted as if the cavity was an enclosed volume with six walls. The possible frequencies of room modes are given by

$$f_c = \frac{c}{2}\sqrt{\left[\left(\frac{n_x}{L_x}\right)^2 + \left(\frac{n_y}{L_y}\right)^2 + \left(\frac{n_z}{L_z}\right)^2\right]} \qquad (7)$$

where n_x, n_y, and n_z can independently take on integer values 0, 1, 2,...∞. Thus, many modes are possible.

Measurements of cavity pressure modes were made with microphone no. 3 by probing the cavity interior during resonance. Figure 16 is a typical time trace at one point in the 305-mm-deep cavity during a resonant condition. The cavity was covered by screen no. 1. The rms acoustic pressure variation with vertical position in figure 17(a) shows that there was very little pressure variation in the vertical direction. The cavity pressure modes varied only in the horizontal plane. Thus, $n_z = 0$ in all cases. This indicates that the excitation from the screen was uniform in the vertical direction.

Figure 17(b) shows the rms acoustic pressure variation in the depth (cross-stream) and width (streamwise) directions. The pressure varied in both directions, but a clear resonance mode cannot be identified for two reasons. 1) The resonance frequency was approximately 3470 Hz, which corresponded to an acoustic wavelength of 98 mm. Since the measurements were made at relatively widely spaced positions, as shown on the figure, the successive peaks and valleys in the mode were not identified. In fact, the 12.7-mm-diameter microphone occupied a significant portion of the wavelength, which would have made it difficult to track the pressure variations between nodes. 2) The following modal analysis indicates that the acoustic wave was reflecting obliquely from adjacent walls in the horizontal plane. The surveys that used data for only the depth or width direction could not track the mode properly.

Despite the difficulty of identifying the modes with the cavity surveys, equation 7 makes it possible to match measured resonance frequencies against all possible modal frequencies. For example, table 2 lists the possible (n_x, n_y, 0) modes for the cavity geometry and temperature corresponding to the data of figure 17(b). (The cavity temperature is used to compute sound speed.) The measured resonance tone of 3470 Hz matches, to within experimental accuracy, the (6, 2, 0) mode or $n_x = 6$, $n_y = 2$, $n_z = 0$ mode at 3474 Hz predicted from equation 7. In this manner, the spectral data were analyzed to identify the excited modes with a reasonable expectation of accuracy.

Note that with modal patterns (n_x, n_y, 0), the pressure fluctuations along the screen will be in phase, even though the amplitude of fluctuations will vary along the screen. Thus, all the orifices will pump air in and out of the cavity in phase. (See Beranek's (1971) plots of pressure contours in a resonant enclosure.)

By comparison with screened cavities, the important resonance modes of shallow open cavities are the first several modes in the streamwise direction (Block, 1977). Those modes are much fewer in number than the number of possible acoustic modes in screened cavities.

Phase Coupling of the Orifice Vortex Shedding and Cavity Tones

Davies (1981) suggested that airflow past a slot in a wall or cavity will generate a vortex sheet and can excite cavity resonances when the ratio of vortex spacing (or wavelength)-to-slot width is 2, 3, 5, 7 and so on. At those conditions, the vortices passing over the cavity will induce flow in and out of the cavity in a periodic manner, which, if the frequency of the induced flow occurs at a cavity modal frequency, will excite resonance. Similarly, the data from this experiment indicate that screen covered cavities will resonate only when the ratio of vortex sheet wavelength-to-hole spacing, λ_v/ℓ, has a magnitude given by

$$\frac{\lambda_v}{\ell} = 0.25, \quad 0.5, \quad \text{or} \quad 1.0 \qquad (8)$$

The vortex wavelength or spacing is defined as

$$\lambda_v = \frac{U_c}{f_v} \qquad (9)$$

The value of λ_v/ℓ cannot be greater than 1.0 since the air is pumped out of the screen orifices simultaneously during resonance. Hence, the vortices cannot be farther apart than one hole spacing. A value of $\lambda_v/\ell = 0.25$ gave a weak resonance compared to the other two values in equation 8.

A discussion of equation 8 follows. At the ideal condition of $\lambda_v/\ell = 1.0$, the vortex ejected from an orifice during cavity resonance will generate a normal velocity at the screen that will oscillate in phase with the acoustic pressure fluctuations at the screen as illustrated in figure 18. At one part of the cycle, the induced inflow velocity at each orifice will coincide with a low acoustic pressure in the cavity near the orifice, which results in an injection of energetic flow into the cavity. Later in the cycle, the induced velocity from the vortices will generate an outflow at the same time the cavity pressures are positive and are also inducing an outflow. At that time, the outflow will create a new vortex which will be overtaken in phase with the vortex that arrived from the upstream hole one cycle previously. Similar arguments hold for vortices shed two or more cycles previously. This interaction will provide the continuous flow of energy necessary to sustain cavity resonance. If the interaction of the vortex sheet and cavity acoustic pressures are interrupted in any way, resonance will not occur. The strong correlation between cavity pressures and the periodic hot-wire signal in the wake of an orifice during resonance was measured (fig. 19). Such a strong correlation verifies that the signals are coupled.

With the relationships for vortex shedding rate, f_v, from equations 1 and 2, the ratio of vortex wavelength to hole spacing can be written as

$$\frac{\lambda_v}{\ell} = \frac{U_c \frac{d}{\ell}}{U_o St} = \frac{U_c \frac{d}{\ell}}{U_o(-0.01 + 0.10\,d)} \qquad (10)$$

Thus, for a given ratio of convection speed to free-stream velocity, U_c / U_o, the key parameter that defines the vortex/cavity phase correlation for resonance, λ_v/ℓ is only a function of perforation diameter and spacing. This ratio λ_v/ℓ will be called the "phase coupling parameter." Since U_c / U_o is probably constant for a wide range of airspeeds, equation 10 indicates that the phase coupling parameter and, by implication, the resonance or nonresonance of the cavity depends only on perforation geometry. Hence, if a cavity-screen geometry does not resonate at a given speed (above the oscillation threshold), it will not resonate at any speed. This is a very important factor in the design of screened cavities.

Effect of Hole Diameter and Spacing on Resonance

Eight perforation patterns listed in table 1 were tested. By changing hole diameter, hole spacing, flow speed, and cavity depth, the key parameters affecting resonance could be evaluated. The results of perforation variation fell into two general categories. 1) Those perforations which created a phase coupling parameter whose magnitude was close to 0.25, 0.5, or 1.0 generated cavity resonance. 2) Those perforations which produced parameters not close to those values did not generate tones. Of those configurations tested which resonated, screen no. 1 with 3.18-mm diameter holes generated the loudest tones. Screens that had 1.59 mm diameter holes generated the weakest tones, probably because of viscous losses at the orifices.

Figure 20 illustrates the basic mechanisms affecting the frequency at which resonant tones are generated. The data were from microphone no. 2. The dominant tone at 9410 Hz is not close to the predicted orifice vortex shedding rate of 8910 Hz from equations 1 and 2. However, at the resonant frequency of 9410 Hz, the phase coupling parameter is 0.5, which is ideal for resonance because the vortex hole interaction and cavity pressure fluctuations are in phase. So, the cavity forced the vortices to shed at a rate different from the natural shedding rate estimated from equations 1 and 2. The resonance at 9410 Hz corresponds to the (8, 6, 0) cavity mode. A weaker tone was generated at twice the dominant frequency or 18,820 Hz, which corresponds to the (16, 12, 0) mode and a phase coupling parameter of 0.25. In addition, there was a tone generated at 10,500 Hz which corresponds to the (9, 6, 0) mode, the next highest depth mode relative to the dominant one (i.e., n_x increased by one). In the latter case, the phase coupling parameter was slightly off optimum (0.45), but was close enough to excite resonance in the (9, 6, 0) mode. As airspeed increased, the (9, 6, 0) tone became the dominant tone.

1.59-mm-diameter holes– Four screens were evaluated with 1.59-mm hole diameters and hole spacings ranging from 4.37 to 8.73 mm (table 1). The ratio of hole diameters to hole spacings, d/ℓ 19 , varied from 0.18 to 0.36. Figures 21(a)-(d) illustrate radiated noise spectra for a flow speed of approximately 67 m/sec. For comparison, acoustic spectra are shown from cavities covered by

screen no. 1, which had 3.18-mm-diameter holes and generated strong tones.

None of the hole spacings generated consistent cavity resonances except the spacing of 6.35 mm in screen no. 5 (fig. 21(c)). Assuming a normalized convection speed of 0.60, the 6.35-mm hole spacing created a phase coupling parameter of 1.0, which satisfies equation 8. The other hole spacings created phase coupling parameters, which did not correspond to the values of equation 8. (The weak tones in the spectra of the four figures were either wind tunnel background noise or nonresonant cavity tones.) Note that screens no. 1 and no. 5 had equal open areas (4.9 %) and equal ratios of hole spacing-to-diameter (0.25) (table 1).

It also important to note that cavity resonance induced by the screens with 1.59-mm-diameter holes was weaker than from the screen with 3.18-mm-diameter holes (fig. 21(c)). It is known that the energy of air pumping in and out of orifices is dissipated by viscous stresses at the edge of the holes (Cummings, 1981). Hence, large holes would be less affected by edge effects than small holes. This transfer of fluid motion energy into heat by the action of viscosity at the orifice is the fundamental mechanism of a sound absorbing Helmholtz resonator. A screened cavity is similar in many respects to a Helmholtz resonator, even if the resonance modes are dissimilar.

3.18-mm-diameter holes– Both screens no. 1 and no. 2 had 3.18-mm-diameter holes, but the hole spacing on screen no. 2 was 9.53 mm as compared to 12.7 mm for screen no. 1. Figure 22(a) shows that at 43 m/sec airspeed, the cavity covered by screen no. 1 resonated quite well, whereas the cavity covered by screen no. 2 had not yet begun to resonate well. As airspeed increased to 48 m/sec, screen no. 2 started to generate tones as shown in figure 22(b). Using a normalized convection speed of 0.65, the computed phase coupling parameter, λ_v/ℓ of screen no. 1 was close to the ideal of 0.5 as compared to 0.72 for screen no. 2 at this condition. This value of phase coupling for screen no. 2 contradicts the requirement of equation 8 unless the convection speeds for the vortices on the two screens were different.

The average convection speed of the vortices from one orifice to the next may change with hole spacing. Consider the boundary-layer profile in figure 15(b). In the lower part of the boundary layer, the velocity gradient is quite steep. A small change in height in the boundary layer results in a large change in velocity. Thus, as the vortices rise in the boundary layer, they will accelerate. Since each vortex started as a ring vortex, the self-induced velocities would cause the vortex to rise as they move downstream. It follows, therefore, that the vortices which have to travel farther to reach the next orifice would accelerate more so that the average convection speed would be greater than that of vortices traveling a shorter distance. An average convection speed of 0.65 U_0 was used for screen no. 1, which had 12.7-mm hole spacing. If an average convection speed around 0.50 U_0 is used for screen no. 2, which had 9.53-mm hole spacings, the resulting phase coupling parameter for the data from screen no. 2 (figs. 22(b) and (c)) satisfies the criterion of equation 8.

At U_0 = 80 m/sec (fig. 22(c)), both screen-induced resonances were similar. Although resonance from screen no. 2 was louder, the resonance from screen no. 1 was split between two modes, so the acoustic energy was actually higher than it was in the single mode of screen no. 2. The distribution of energy among the possible modes depends on temperature, which was not constant from run to run. Note that the broadband noise from screen no. 1 was consistently higher than screen no. 2 despite the fact that screen no. 1 had the fewer number of holes; the reason for this has not been determined. Tones in the spectra from both screens were also strong at 91 m/sec.

Screen no. 3, which also had 3.18-mm-diameter holes, did not excite cavity resonance despite the relatively close hole spacing of 6.35 mm (d/ℓ = 0.5) as shown in figure 23. At other speeds, weak tones were observed from screen no. 3. Once again, it is clear that because the screen no. 3 phase coupling parameter value was outside the range given by equation 8, strong resonance was suppressed. Thus, decreasing the hole spacing uncoupled the aeroacoustic interaction, which was contrary to expectations.

6.35-mm-diameter holes– The largest hole diameter investigated (screen no. 8) did not generate resonant tones at 43 m/sec airspeed because of the value of the phase coupling parameter (fig. 24(a)). Similar results are shown in figure 24(b) for 75 m/sec airspeed.

The results of this section are summarized in table 3, which shows the role of perforation geometry and phase coupling parameter on tone generation. These results indicate that the simplest way to avoid cavity resonance is to avoid orifice diameter-to-spacing ratios around 0.25. Ratios around 0.50 would be better.

Cavity Resonance Versus Airspeed

As airspeed over a resonating cavity was gradually increased, acoustic energy decreased in some modes and increased in others. The tones did not shift smoothly with airspeed. This characteristic of resonant cavities has been documented for open cavities by many others (for example, De Metz and Farabee (1977)).

Figures 25(a) - (c) show typical spectra measured at airspeeds of 48, 54, and 59 m/sec. At 48 m/sec (fig. 25(a)), two strong tones were generated near 5 kHz. As the airspeed was increased to 54 m/sec (fig. 25(b)), the tone at 4700 Hz was attenuated, and new tones between 5 and 6 kHz grew. At 59 m/sec, the tone at 6900 Hz become the dominant tone. The modes for all the tones are listed on the figures and were determined from the list of all possible modes using equation 7. (Table 2 gives an example of all possible modes for one test condition.) To the listener, this variation of tonal frequency with airspeed was disjointed. A condition could be reached where the dominant tone was almost pure. As airspeed changed, the energy that was building in other modes caused the sound to become harsh. At some point the strongest tone would seem to jump to a new frequency.

By plotting the frequency of the dominant tone as it increased with airspeed, the stepwise frequency variation is illustrated (figure 26(a)). The data were recorded with screen no. 1 installed over a 152-mm-deep cavity. The data show that the dominant tone frequency would remain fairly constant over a range of around 5 m/sec, then increase as airspeed continued to rise. Figure 26(b) shows that for the same data the tone amplitude increased to a maximum near 5 kHz, when the airspeed reached 48 m/sec and remained fairly constant over the range of airspeeds evaluated. The first tone detected with this geometry was at an airspeed of U_o = 15 m/sec.

Open Cavity Oscillations and Depth Effects

Screened and open cavities (in which the screen is removed) resonate at completely different frequencies. For a 152-mm cavity depth and an airspeed of 61 m/sec, screen no. 1 generated a resonance at 5910 Hz, whereas the same cavity without a screen resonated at 300 Hz (fig. 27(a)). Clearly, the screen suppresses the large-scale, low frequency fluid oscillation characterized by a single vortex in the open shallow cavity which is driven by the external flow (Heller et al., 1971). The screen changes the entire aeroacoustic mechanism such that the cavity pressure fluctuations become acoustic rather than hydrodynamic. The screened cavity acoustic modes are driven at relatively high frequencies by vortex shedding at the screen holes. The large-scale hydrodynamic fluctuations in the open shallow cavity occur at relatively low frequencies.

For a cavity depth of 302 mm, the screened cavity resonated at 6310 Hz, and the open cavity resonated at 200 Hz (fig. 27(b)). Thus, deepening the cavity caused the screen induced resonance frequency to increase, whereas the open-cavity resonance frequency decreased. This occurred because, in the case of the screened cavity, the increased depth required a higher order acoustic mode to fit in the depth dimension. The excitation was unchanged, so the resonance frequency does not change dramatically. On the other hand, the deeper open cavity allows a larger eddy to form and rotate at a slower rate.

The open cavity resonance agrees with the third cavity length mode measured and predicted by Block (1977). The predicted open cavity oscillation rate from Block is

$$f_v = \frac{n_y U_o}{L_y\left[\frac{1}{U_c/U_o} + M\left(1 + \frac{0.514}{L_y/L_x}\right)\right]} \qquad (11)$$

For the parameter values corresponding to the configuration and flow conditions of figure 27(b), equation 11 gives a value of 204 Hz if $n_y = 3$ and $U_c/U_o = 0.6$. (That convection speed for open cavities comes from Block.) The predicted frequency is close to the measured frequency of 200 Hz for the open cavity oscillation. Note that equation 11 predicts a decrease in frequency with an increase in cavity depth, which is consistent with our experimental results.

Multiple Cavities

It was discovered that two cavities facing each other across the airstream caused the amplitude of the resonance to intensify (fig. 28). The data were acquired by measuring the cavity noise with two vanes and cavities installed, and then alternately covering and uncovering one screen with a solid plate. The acoustic energy from one cavity successfully amplified the resonance of the other cavity. Although two noise sources would be expected to be 3 to 6 dB louder than one source, the measured noise increase due to uncovering the second cavity was as much as 14 dB. Furthermore, figure 28 shows that a mode was excited at 3 kHz by two cavities that was not excited at all with only one cavity operative. This result is in agreement with the observation that silencers composed of numerous cavities can generate very strong tones, even with small orifices (Soderman, 1981 and 1982).

In an attempt to stimulate resonance in a cavity covered by screen no. 4, the right vane was replaced with a horn and driver on the floor and aimed at the vane. Screen no. 4 did not generate tones during the studies with airflow alone. Nor would it support resonance in the presence of airspeed and loud tones from the loudspeaker. The loudspeaker was driven with tones at frequencies where resonance might be expected. Cavity depths of 152 and 302 mm were used. This nonresonance supports the idea that cavity resonance can be sustained only by coupling of the cavity pressure oscillations and aerodynamic perturbations on the screen.

CONCLUSIONS

This report describes an experimental study in the Ames 7- by 10-Foot Wind Tunnel of screen-covered cavities exposed to airflow tangent to the screen. Aerodynamic and acoustic measurements were made to identify the mechanisms responsible for cavity resonance and to find ways to uncouple the feedback interactions. The study was made at airspeeds from 0 to 100 m/sec. The 457-mm-long by 1.09-m-high rectangular cavities had length-to-depth ratios greater than one, which is characteristic of shallow cavities. The screens used to cover the cavities were thin metal plates perforated in straight rows and columns. The perforation holes had diameters ranging from 1.59 to 6.35 mm and had porosities from 2.6% to 19.6%.

Hot wire and acoustic measurements indicated that strong cavity acoustic resonances were created by screen orifices which shed vortices that coupled with cavity pressure oscillations. It was deduced that if the vortices propagated to the next downstream orifice in phase with the cavity oscillations, the velocities induced through the orifices would sustain cavity resonance. The dominant resonance occurred at a cavity mode that was close to the natural shedding rate of the orifices. Weaker tones were observed in nearby modes and at frequencies which were integer multiples of the strongest resonant frequency.

The aeroacoustic coupling depends on several parameters: free-stream velocity, cavity acoustic modes, screen hole diameter, hole spacing, and the vortex convection speed. By choosing a hole pattern with correct spacing, the shed vortices cannot pass from one hole to another in time to reinforce the cavity oscillations. The estimation of convection speed depends on the height at which the vortices propagate in the boundary layer. Some of the measurements indicated that the convection speed varied with orifice diameter and distance of vortex propagation, both of which affect vortex height in the boundary layer.

The primary finding of the study was that shallow cavity resonance can be eliminated by the proper choice of screen hole pattern regardless of airspeed. The criterion for resonance or nonresonance is formulated in terms of a phase coupling parameter, which is equal to the ratio of vortex wavelength-to-hole spacing. Resonance will occur when that parameter is equal to 0.25, 0.50, or 1.0. For the cavities studied here, loud tones were induced by screen no. 1 at all airspeeds greater than 30 m/sec. That screen had 3.18-mm-diameter holes on 12.7 mm spacings, which resulted in a ratio of hole diameter-to-spacing of 0.25. Screens with hole diameter-to-spacing of 0.50 created phase coupling parameters that did not permit strong cavity resonance over the complete range of airspeeds evaluated (0 to 100 m/sec). Thus, hole spacings which prevented cavity resonance did not depend on airspeed. However, weak nonresonant tones were observed in all the cavities at some flow conditions.

The screened cavities that did resonate did so at much higher frequencies than the equivalent open cavity. That is because the classical large eddy rotation in the open cavity is replaced by a cavity acoustic resonance triggered by orifice vortex shedding, a phenomenon that occurs at the relatively small scale of the orifices. Hence, the excitation typically has a high frequency. It was also shown that small orifices tend to weaken the aeroacoustic interaction, probably because of viscous losses at the orifices.

The range of cavity and screen geometries for which the results of this study can be applied is not known. For example, in the extreme case of a cavity with a single hole of adequately large size, cavity resonance can occur. That aeroacoustic mechanism is different from that of a screened cavity (as already discussed for the case of an open cavity). Thus, hole-to-hole coupling or decoupling in the interface between the cavity and flow field does not always apply.

Ames Research Center
National Aeronautics and Space Administration
Moffett Field, California 94035
January 2, 1990

REFERENCES

Bauer, A. B.; and Chapkis, R. L.: Noise Generated by Boundary Layer Interaction with Perforated Acoustic Liners. AIAA Paper 76-41, AIAA 14th Aerospace Sciences Meeting, Wash. DC, Jan. 1976.

Baumeister, K. J.; and Rice, E. J.: Visual Study of the Effect of Grazing Flow on the Oscillatory Flow in a Resonator Orifice. NASA TM-X-3288, Sept. 1975.

Beranek, L. L.: Noise and Vibration Control. ch. 8, p. 210. McGraw-Hill Book Co., New York, 1971.

Block, P. J. W.: Measurements of the Tonal Components of Cavity Noise and Comparison With Theory. NASA TP-1013, Nov. 1977.

Cummings, A.: High-Amplitude Acoustic Power Losses in Perforated Materials. A82-24600, Paper 81-WA/NCA-10, ASME Winter Annual Meeting, Wash. DC, Nov. 1981.

Davies, P. O. A. L.: Flow-Acoustic Coupling in Ducts. J. Sound and Vib. vol. 77, 1981, p. 191-209.

De Metz, F. C.; and Farabee, T. M.: Laminar and Turbulent Shear Flow Induced Cavity Resonances. AIAA Paper 77-1293, AIAA 4th Aeroacoustics Conf., Oct. 1977.

Dougherty, N. S. Jr.; Anderson, C. F.; and Parker, R. L. Jr.: An Experimental Study of Edgetones from Perforated Wind Tunnel Walls. AIAA Paper 76-50, AIAA 14th Aerospace Sciences Meeting, Wash. DC, Jan. 1976.

Heller, H. H.; and Bliss, D. B.: The Physical Mechanism of Flow-Induced Pressure Fluctuations in Cavities and Concepts for Their Suppression. AIAA Paper 75-491, AIAA 2nd Aero-Acoustics Conf., Hampton, VA, Mar. 1975.

Heller, H. H.; Holmes, D. G.; and Covert, E. E.: Flow-Induced Pressure Oscillations in Shallow Cavities. J. Sound and Vib. vol. 18, no. 4, 1971, p. 545-553.

Soderman, P. T.: Test-Section Noise of the Ames 7- by 10-Foot Wind Tunnel No. 1. NASA TM-X-73,134, May 1976.

Soderman, P. T.; and Hoglund, L. E.: Wind-Tunnel Fan Noise Reduction Including Effects of Turning Vanes on Noise Propagation. AIAA Paper 79-0642, AIAA 5th Aeroacoustics Conf., Seattle, WA, March 1979.

Soderman, P. T.: Design and Performance of Resonant-Cavity Parallel Baffles for Duct Silencing. Noise Control Engineering, vol. 17, no. 1, July-Aug. 1981, pp. 12-21.

Soderman, P. T.: A Study of Resonant-Cavity and Fiberglass-Filled Parallel Baffles as Duct Silencers. NASA TP-1970, April 1982.

Schlichting, H. (J. Kestin, transl.): Boundary-Layer Theory, 6th ed., Mc-Graw Hill Book Co., 1968.

Tsui, C. Y.; and Flandro, G. A.: Self-Induced Sound Generation by Flow Over Perforated Duct Liners. J. Sound and Vib. vol. 50, no. 3, 1971, p. 315-332.

Table 1.– Screen Perforation

Screen	Hole diameter,d	Hole spacing, ℓ	Ratio d/ℓ	Open* area
1	3.18 mm	12.70 mm	0.25	4.9%
2	3.18	9.53	0.33	8.7
3	3.18	6.35	0.50	19.6
4	1.59	8.73	0.18	2.6
5	1.59	6.35	0.25	4.9
6	1.59	5.16	0.31	7.4
7	1.59	4.37	0.36	10.4
8	6.35	12.70	0.50	19.6

*Ratio of total hole area to screen area 19 $\times 100 = \frac{\pi d^2}{4\ell^2}$

Table 2.– Cavity Room Modes for Figure 17(b); 302 mm Deep Cavity (63°F); from Equation 7

Room modes															
D, n_x	L, n_y	H, n_z	f_c, H_z	D, n_x	L, n_y	H, n_z	f_c, H_z	D, n_x	L, n_y	H, n_z	f_c, H_z	D, n_x	L, n_y	H, n_z	f_c, H_z
0	0	0	0	0	3	0	1120	0	6	0	2241	0	9	0	3362
1	0	0	565	1	3	0	1255	1	6	0	2311	1	9	0	3409
2	0	0	1131	2	3	0	1592	2	6	0	2510	2	9	0	3547
3	0	0	1696	3	3	0	2033	3	6	0	2811	3	9	0	3766
4	0	0	2262	4	3	0	2524	4	6	0	3184	4	9	0	4052
5	0	0	2827	5	3	0	3041	5	6	0	3608	5	9	0	4393
6	0	0	3393	6	3	0	3573	6	6	0	4066	6	9	0	4776
7	0	0	3958	7	3	0	4114	7	6	0	4549	7	9	0	5193
8	0	0	4524	8	3	0	4661	8	6	0	5049	8	9	0	5636
9	0	0	5090	9	3	0	5211	9	6	0	5561	9	9	0	6100
10	0	0	5655	10	3	0	5765	10	6	0	6083	10	9	0	6579
11	0	0	6221	11	3	0	6321	11	6	0	6612	11	9	0	7071
12	0	0	6786	12	3	0	6878	12	6	0	7147	12	9	0	7573
13	0	0	7352	13	3	0	7437	13	6	0	7686	13	9	0	8084
14	0	0	7917	14	3	0	7996	14	6	0	8228	14	9	0	8602
15	0	0	8483	15	3	0	8557	15	6	0	8774	15	9	0	9125
16	0	0	9048	16	3	0	9118	16	6	0	9322	16	9	0	9653
0	1	0	373	0	4	0	1494	0	7	0	2615	0	10	0	3735
1	1	0	677	1	4	0	1597	1	7	0	2675	1	10	0	3778
2	1	0	1191	2	4	0	1874	2	7	0	2849	2	10	0	3903
3	1	0	1737	3	4	0	2260	3	7	0	3117	3	10	0	4102
4	1	0	2292	4	4	0	2711	4	7	0	3457	4	10	0	4367
5	1	0	2852	5	4	0	3198	5	7	0	3851	5	10	0	4685
6	1	0	3413	6	4	0	3707	6	7	0	4284	6	10	0	5046
7	1	0	3976	7	4	0	4231	7	7	0	4744	7	10	0	5443
8	1	0	4539	8	4	0	4764	8	7	0	5225	8	10	0	5867
9	1	0	5103	9	4	0	5304	9	7	0	5722	9	10	0	6313
10	1	0	5667	10	4	0	5849	10	7	0	6230	10	10	0	6778
11	1	0	6232	11	4	0	6398	11	7	0	6748	11	10	0	7256
12	1	0	6796	12	4	0	6949	12	7	0	7273	12	10	0	7746
13	1	0	7361	13	4	0	7502	13	7	0	7803	13	10	0	8246
14	1	0	7926	14	4	0	8057	14	7	0	8338	14	10	0	8754
15	1	0	8491	15	4	0	8613	15	7	0	8877	15	10	0	9269
16	1	0	9056	16	4	0	9171	16	7	0	9419	16	10	0	9789
0	2	0	747	0	5	0	1867	0	8	0	2988	0	11	0	4109
1	2	0	937	1	5	0	1951	1	8	0	3041	1	11	0	4148
2	2	0	1355	2	5	0	2183	2	8	0	3195	2	11	0	4262
3	2	0	1853	3	5	0	2523	3	8	0	3436	3	11	0	4445
4	2	0	2382	4	5	0	2933	4	8	0	3748	4	11	0	4690
5	2	0	2924	5	5	0	3389	5	8	0	4114	5	11	0	4988
6	2	0	3474	6	5	0	3873	6	8	0	4521	6	11	0	5329
7	2	0	4028	7	5	0	4377	7	8	0	4960	7	11	0	5706
8	2	0	4585	8	5	0	4894	8	8	0	5422	8	11	0	6112
9	2	0	5144	9	5	0	5421	9	8	0	5902	9	11	0	6541
10	2	0	5704	10	5	0	5956	10	8	0	6396	10	11	0	6990
11	2	0	6265	11	5	0	6495	11	8	0	6901	11	11	0	7455
12	2	0	6827	12	5	0	7039	12	8	0	7415	12	11	0	7933
13	2	0	7390	13	5	0	7585	13	8	0	7936	13	11	0	8422
14	2	0	7952	14	5	0	8135	14	8	0	8463	14	11	0	8920
15	2	0	8516	15	5	0	8686	15	8	0	8994	15	11	0	9426
16	2	0	9079	16	5	0	9239	16	8	0	9529	16	11	0	9938

Table 3.– The Variation of Perforation Geometry and Phase Coupling Parameter

	Hole diameter	Hole spacing		Convection speed	Phase coupling parameter	
Screen	d	ℓ	d/ℓ	U_c / U_o	λ_v / ℓ	Comments
1	3.18 mm	12.70 mm	0.25	0.65	0.50[a]	strong tones, $U_o > 30$
2	3.18	9.53	0.33	0.50	0.50[a]	strong tones, $U_o > 40$
3	3.18	6.35	0.50	0.45	0.73[b]	weak tones
4	1.59	8.73	0.18	0.62	0.75[b]	weak tones
5	1.59	6.35	0.25	0.60	1.00[a]	fair tones, $U_o > 40$
6	1.59	5.16	0.31	0.58	1.19[b]	weak tones
7	1.59	4.37	0.36	0.55	1.33[b]	weak tones
8	6.35	12.70	0.50	0.75	0.60[b]	weak tones

[a]Based on frequency of measured tone
[b]Based on frequency of predicted vortex shedding rate

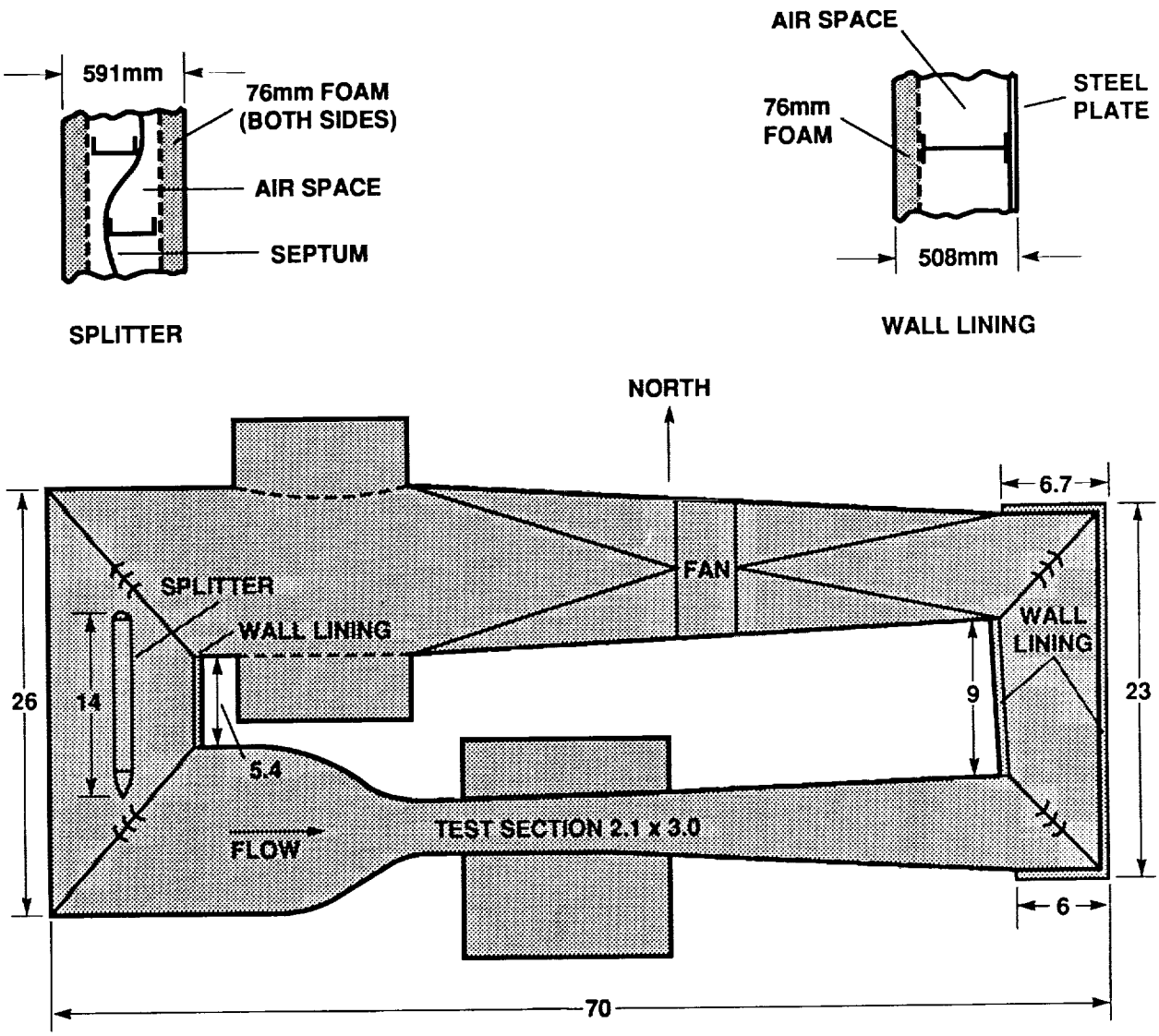

Figure 1.– NASA Ames 7- by 10- Foot Wind Tunnel with acoustic treatment in end legs of circuit.

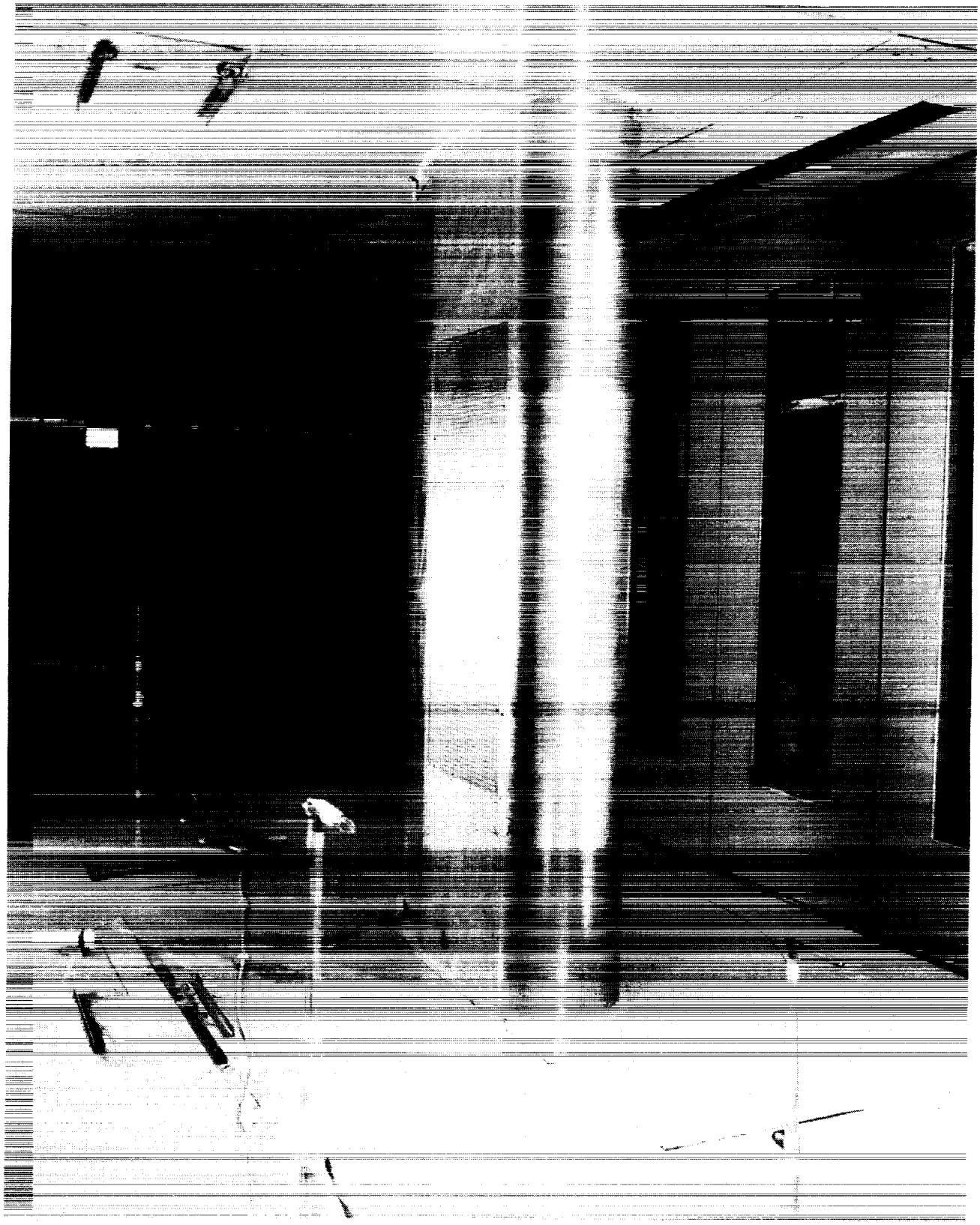

Figure 2.– Photograph of left vane in test section. Microphone no. 1 and pitot-static probe are in foreground. Microphone no. 2 is in background. Note fixtures for attaching right vane to floor and ceiling.

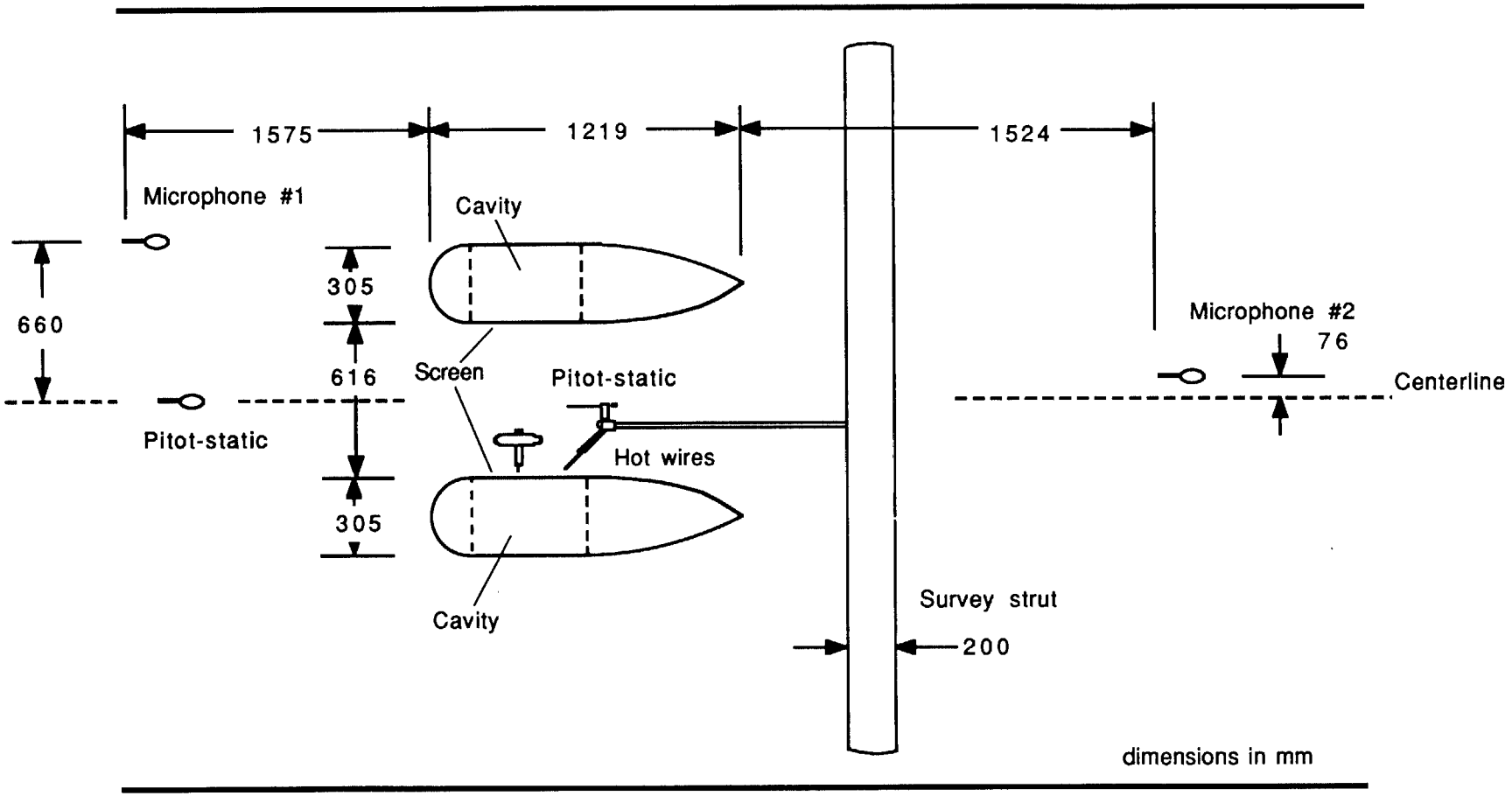

(a) Plan view of 3.05-m-wide test section.

Figure 3.– Vanes, microphones, and flow survey apparatus in test section.

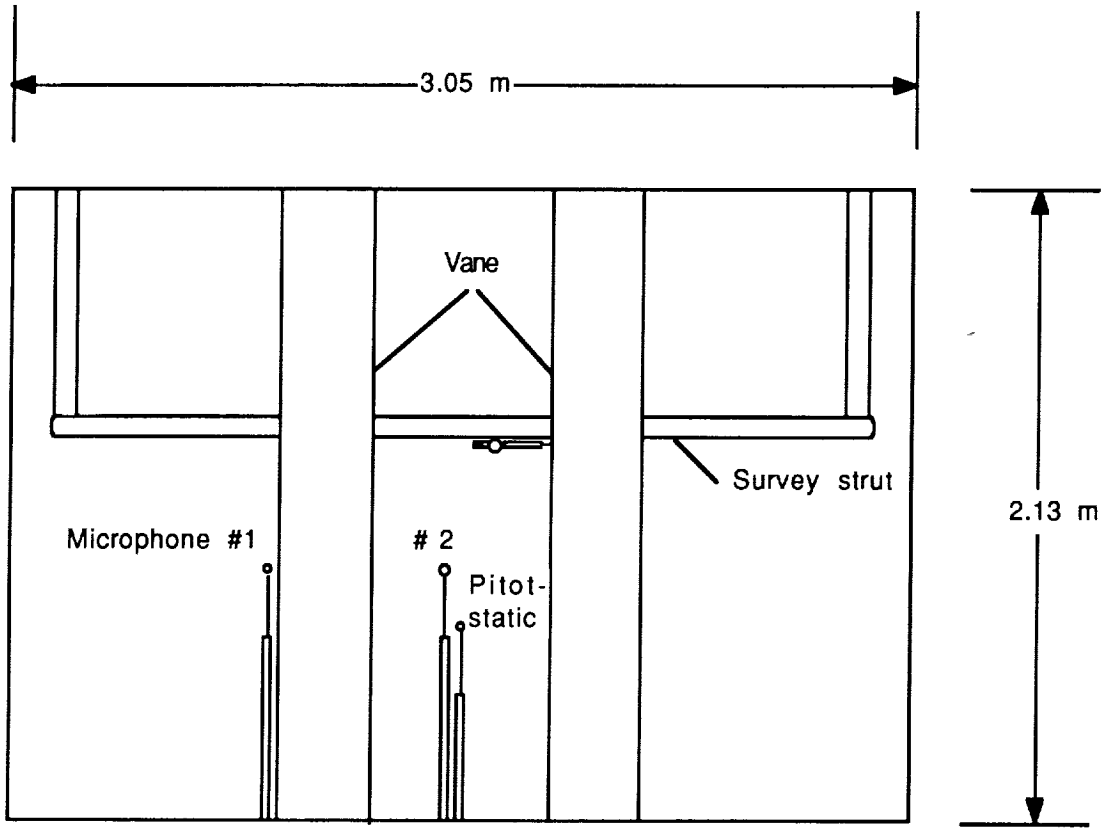

(b) Looking downstream (fixed hot-wire strut not shown).

Figure 3.– Continued.

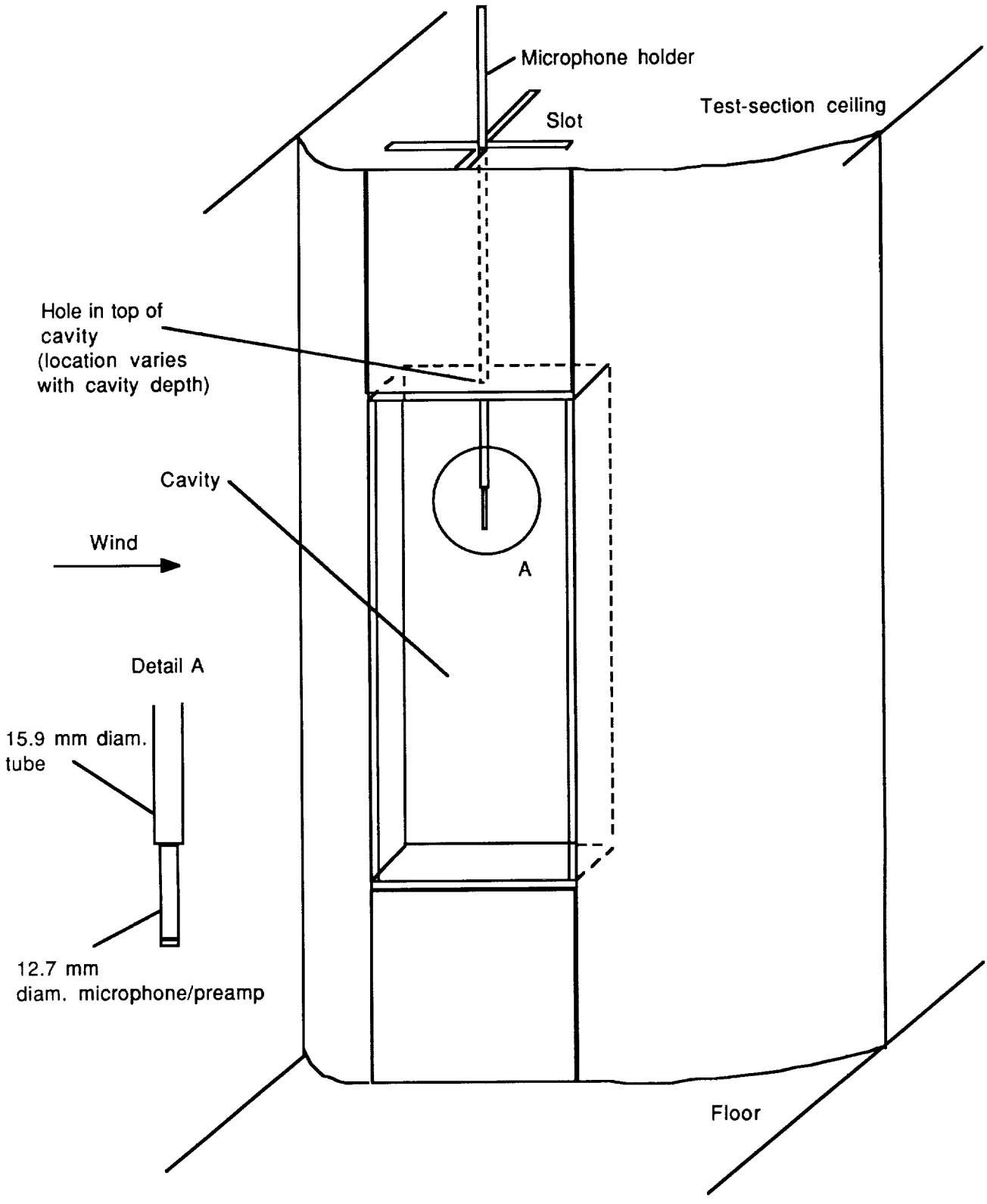

(c) Cavity microphone no. 3.

Figure 3.– Concluded.

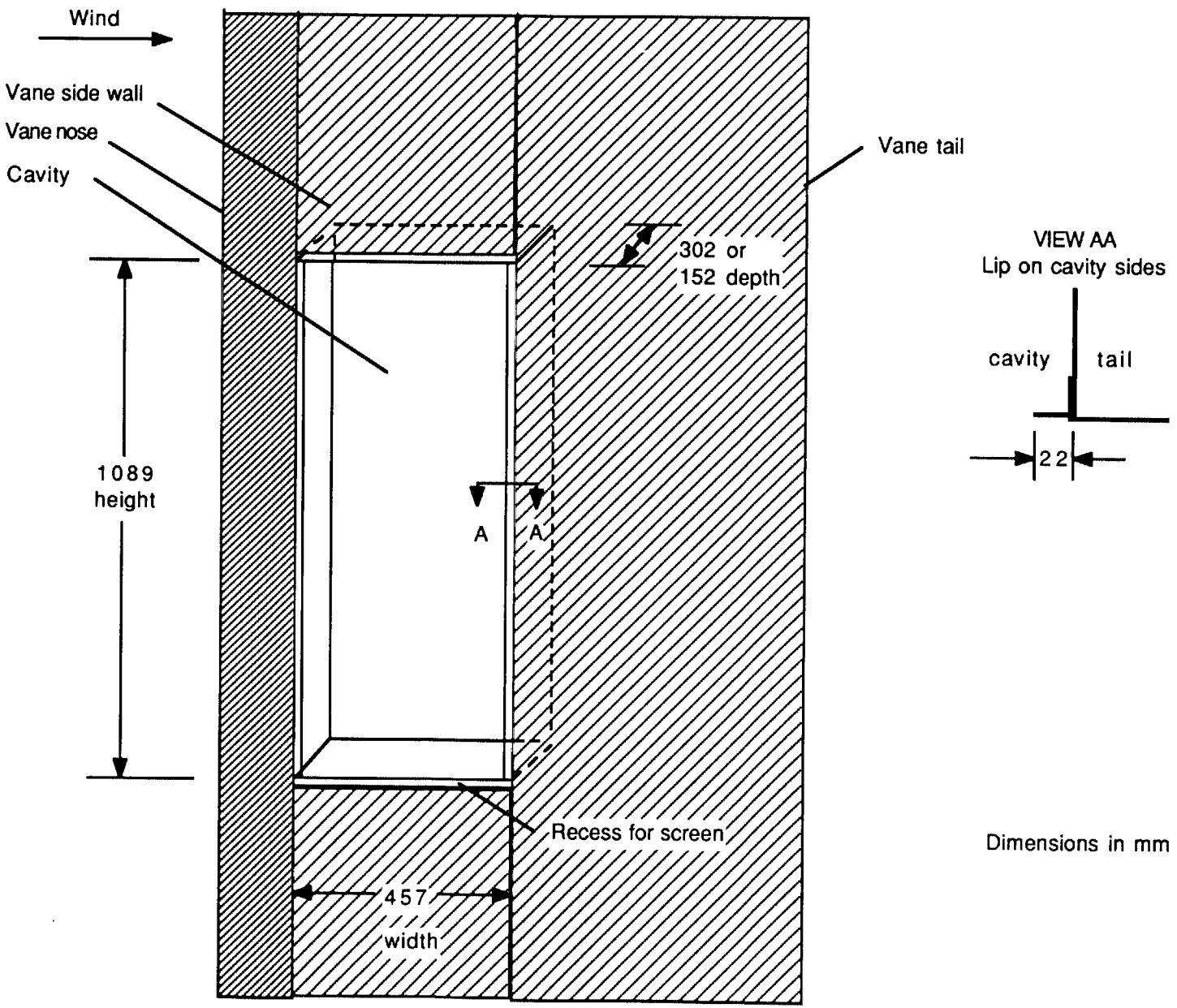

Figure 4.– Cavity geometry.

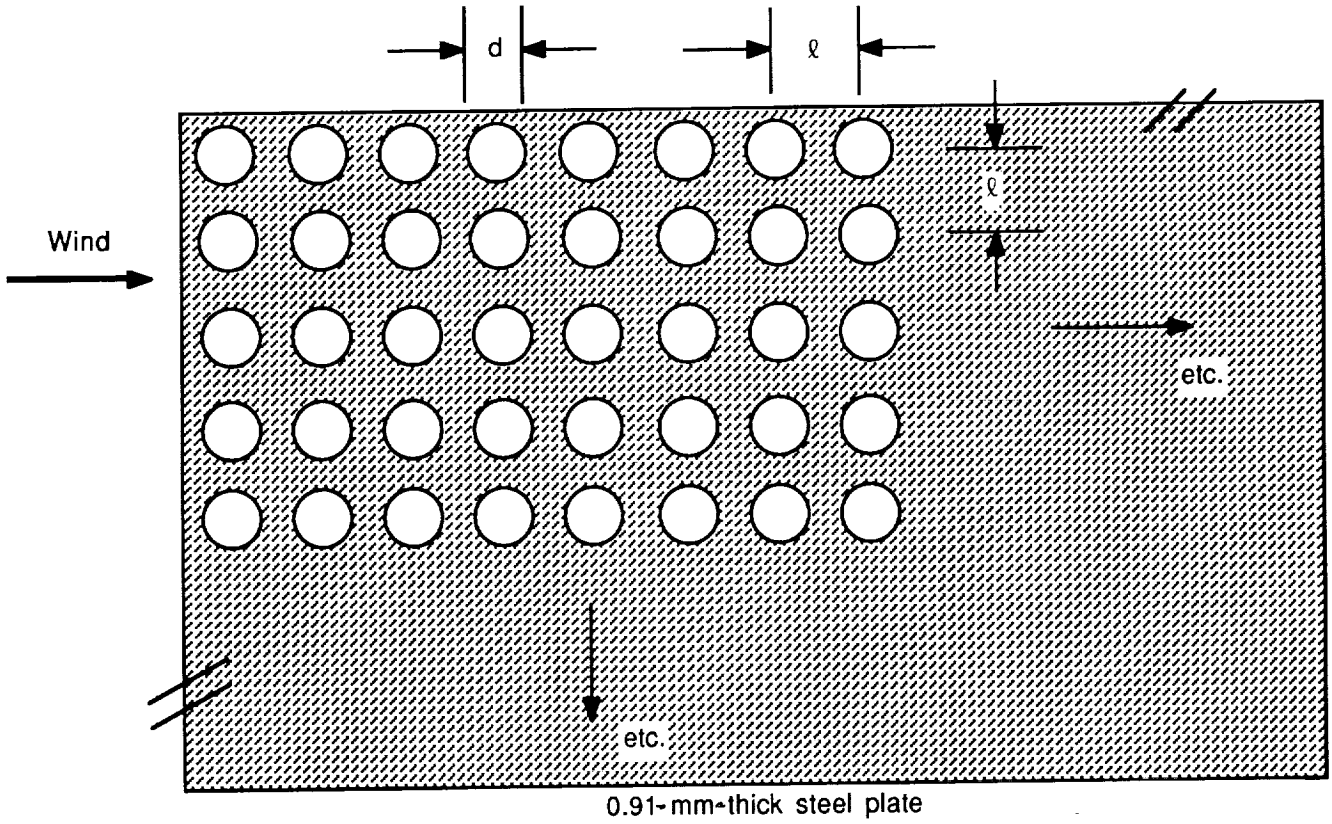

(a) Geometric parameters.

Figure 5.– Typical perforation pattern in cavity cover screen (see table 1 for dimensions).

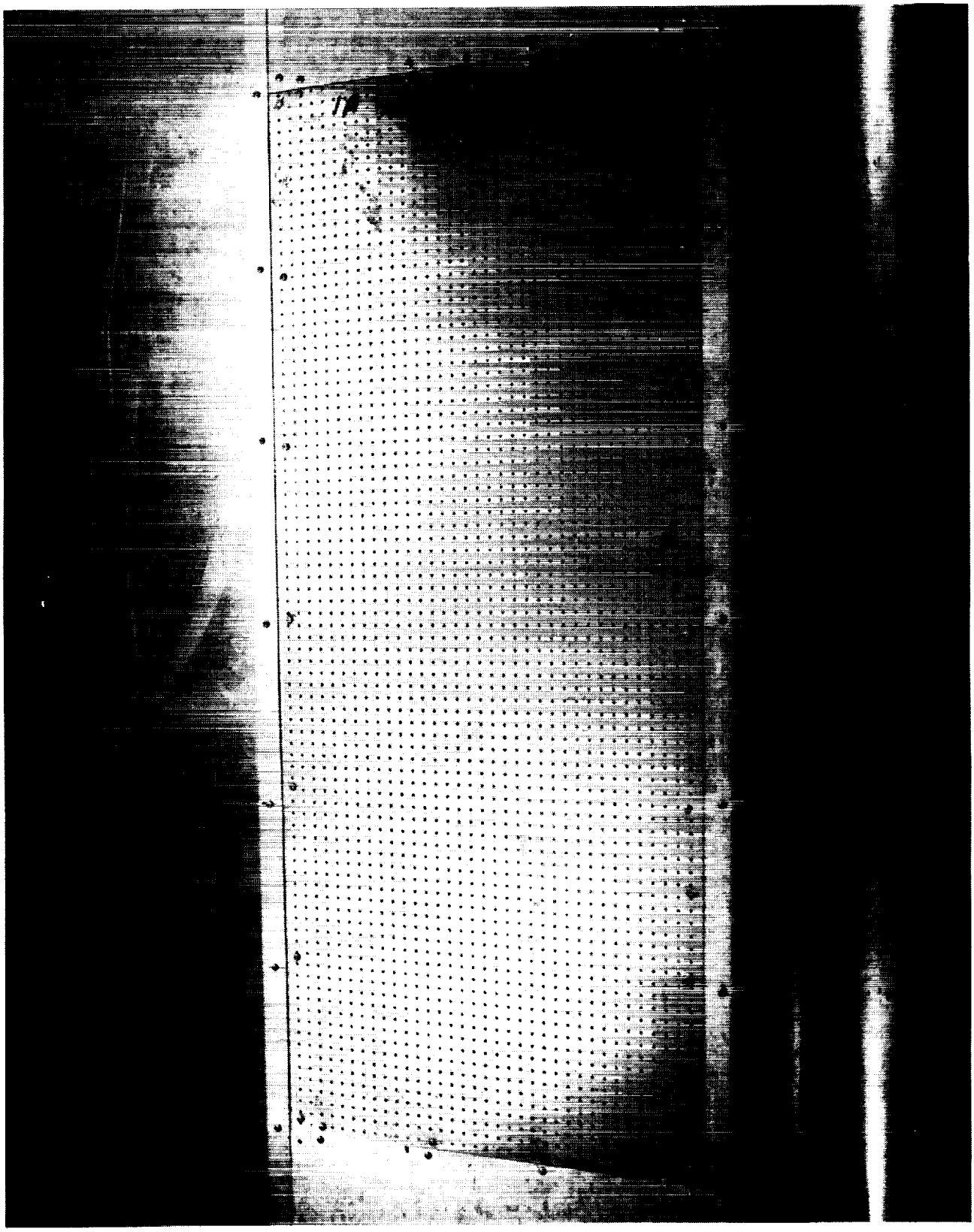

(b) Photo of screen no. 1 mounted on the left vane.

Figure 5.– Concluded.

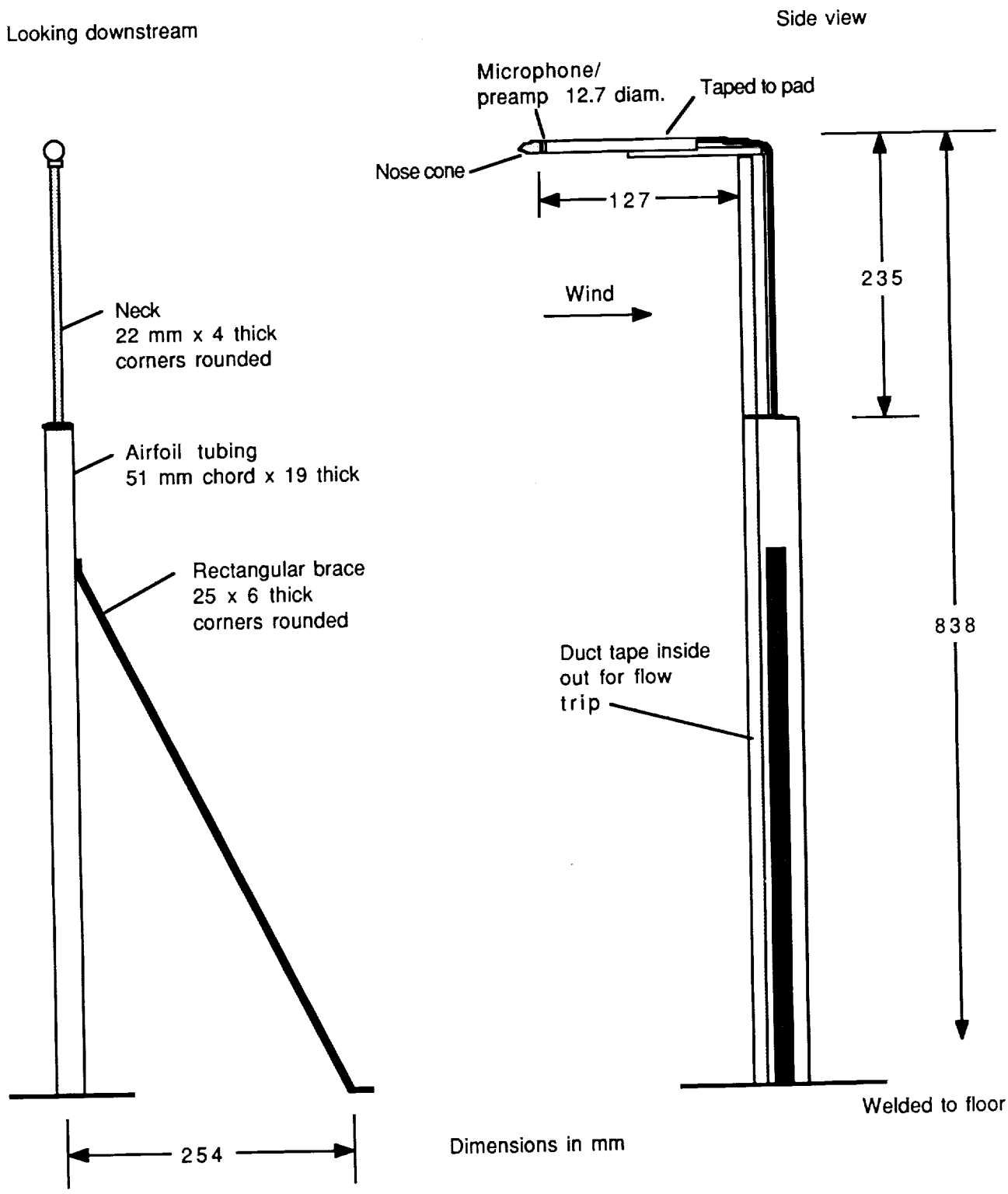

Figure 6.– Strut geometry for microphones no. 1 and no. 2.

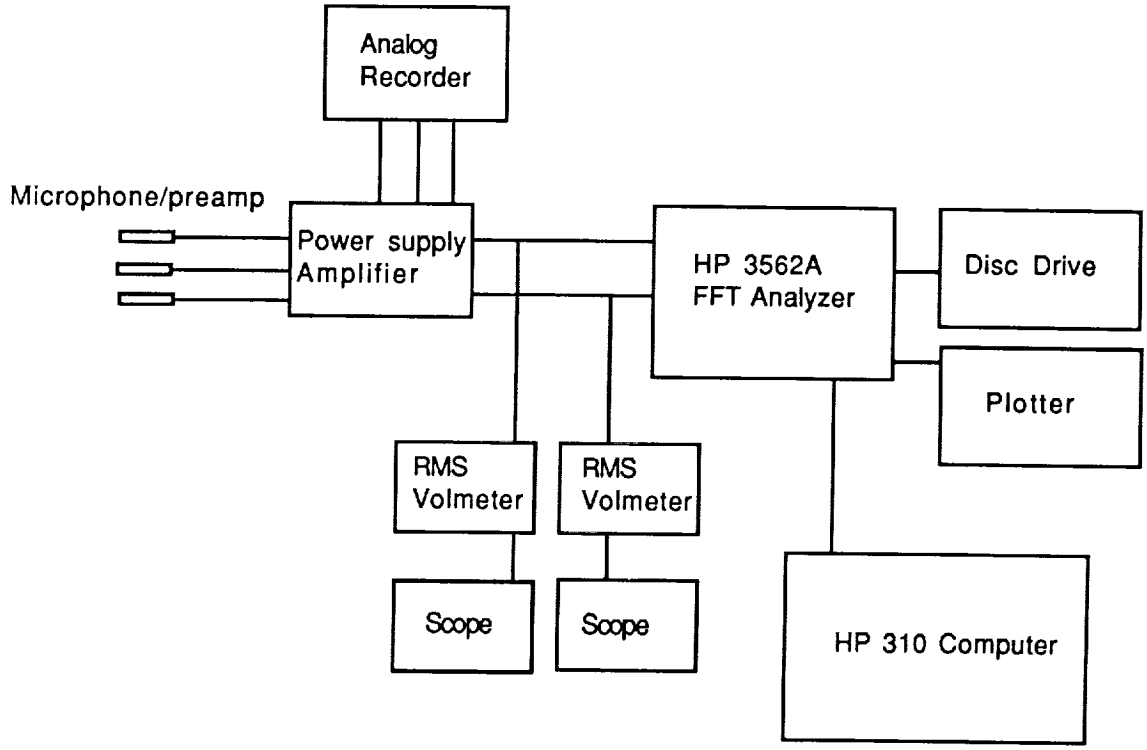

Figure 7.– Acoustic data acquisition and reduction instrumentation. Hot-wire signals were processed with the same analyzer and computer (see fig. 9).

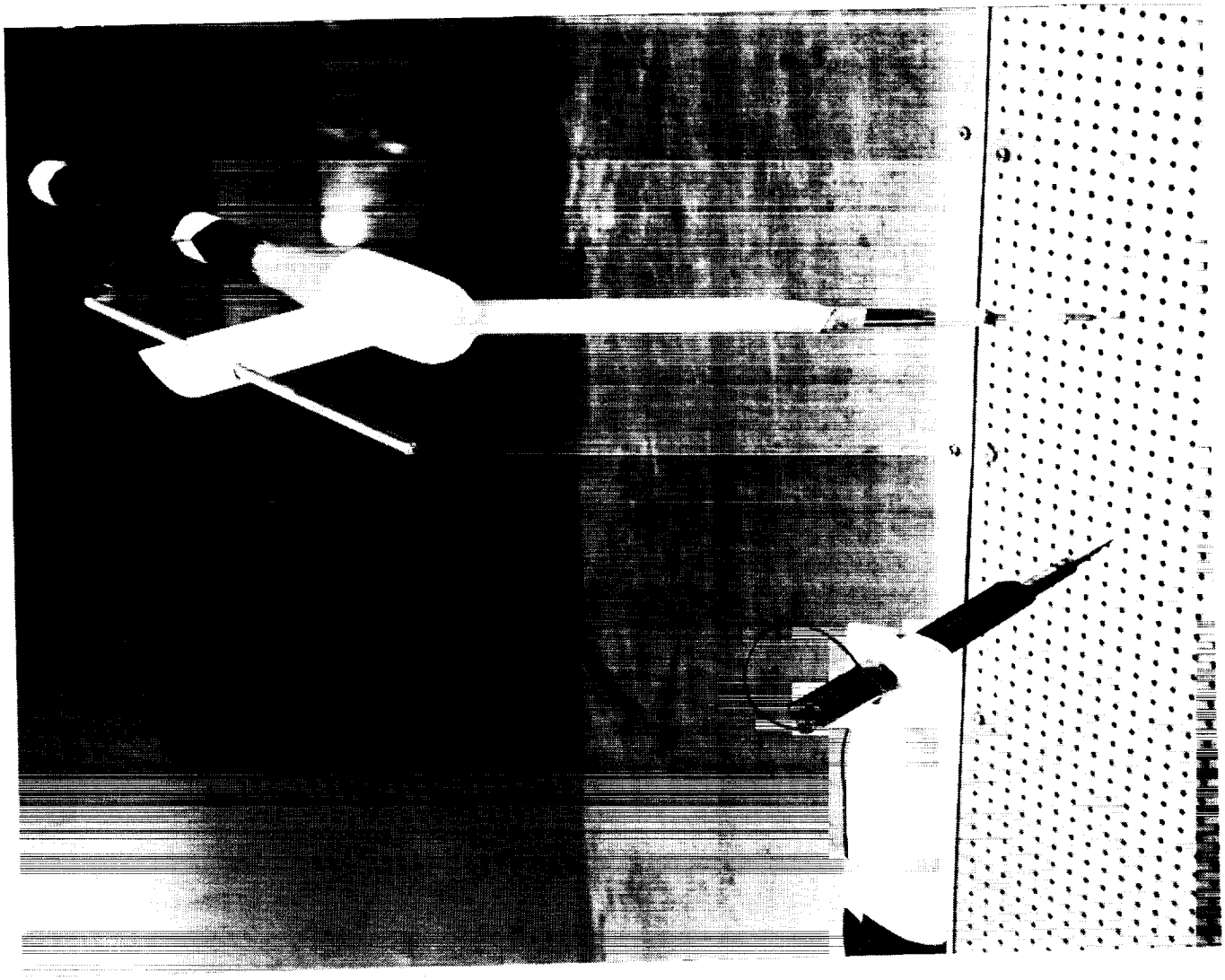

Figure 8.– Flow survey apparatus. Traversing strut in upper part of photo contains pitot-static probe and single hot wire. Fixed strut below holds single hot wire. Flow is from right to left.

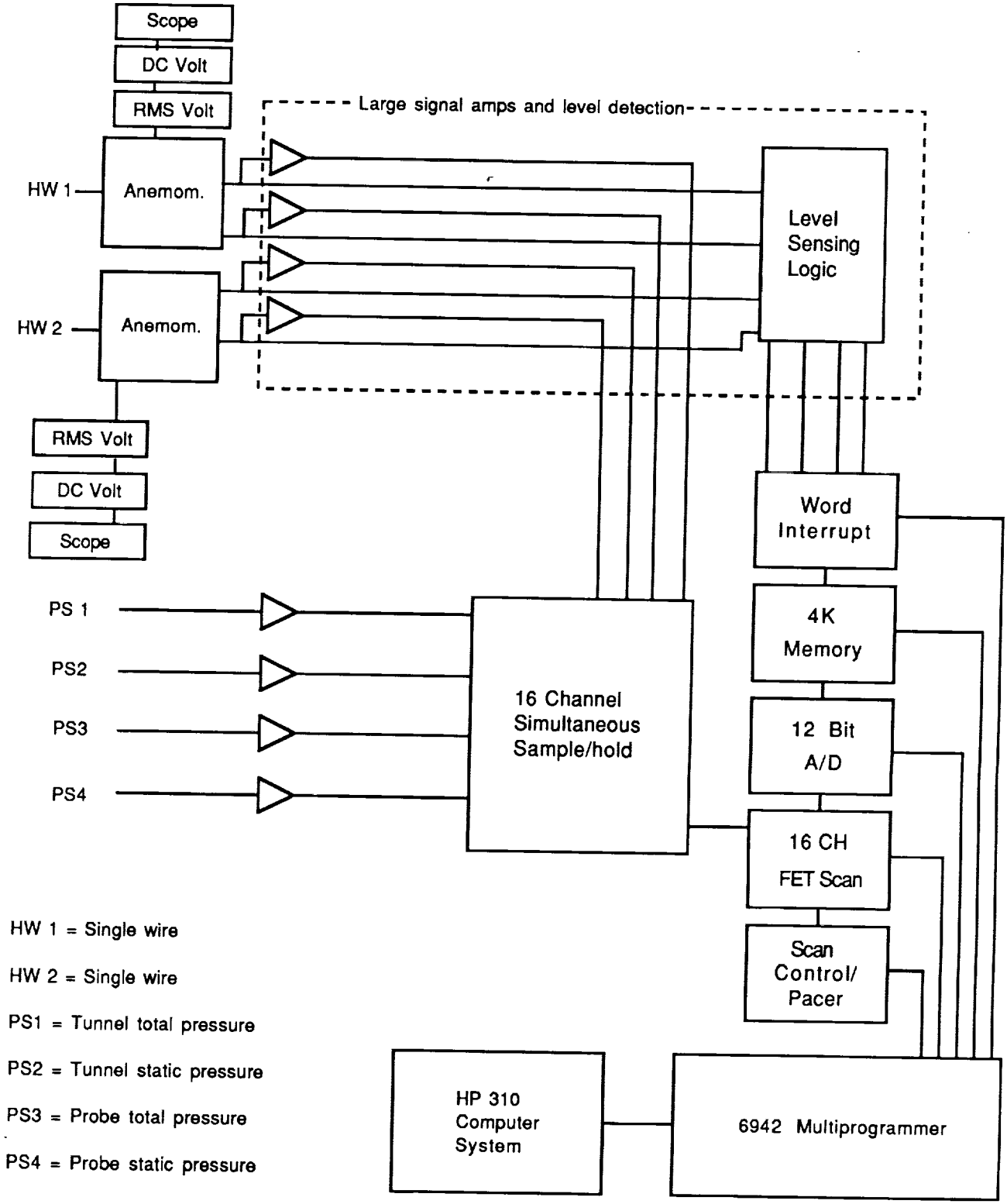

Figure 9.– Hot-wire and pressure instrumentation.

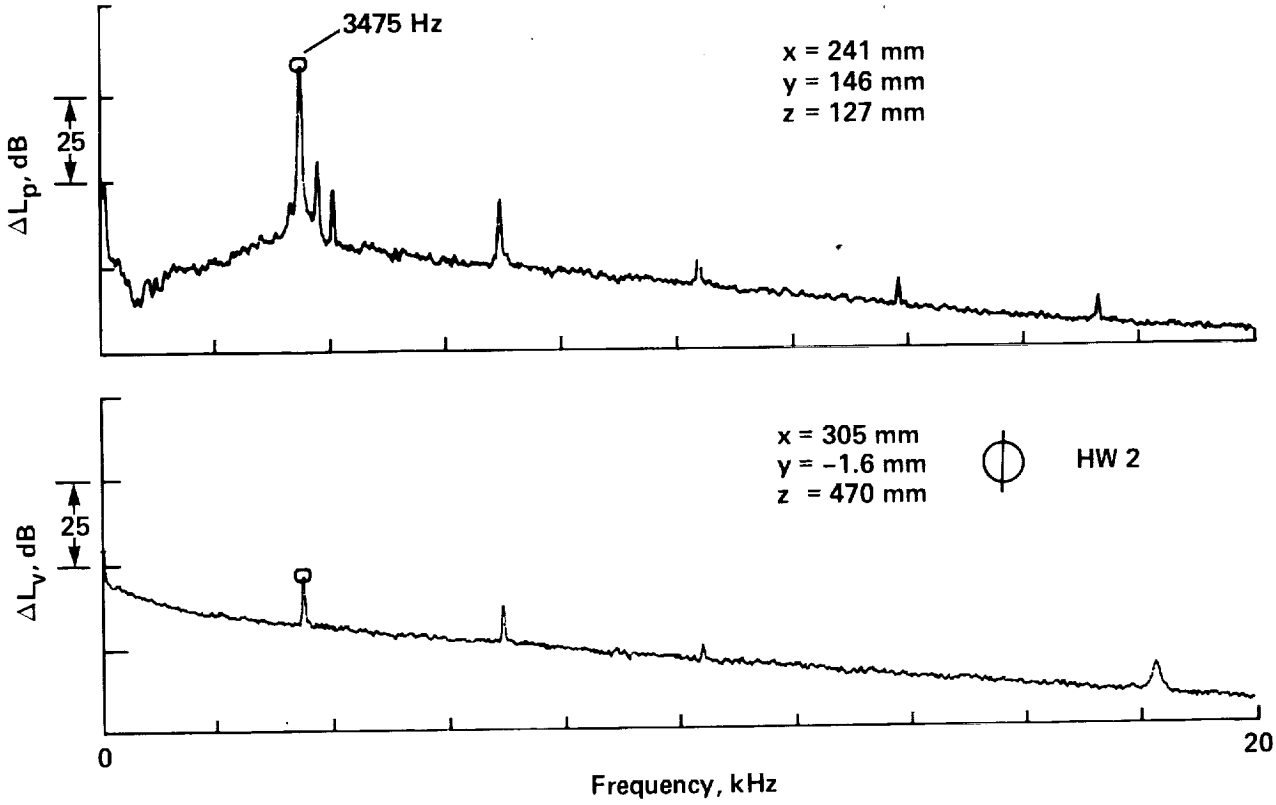

Figure 10.– Spectra from microphone no. 3 in the cavity (upper curve) and hot wire 1.6 mm from screen no. 1 opposite a hole (lower curve). $U_0 = 43$ m/sec.

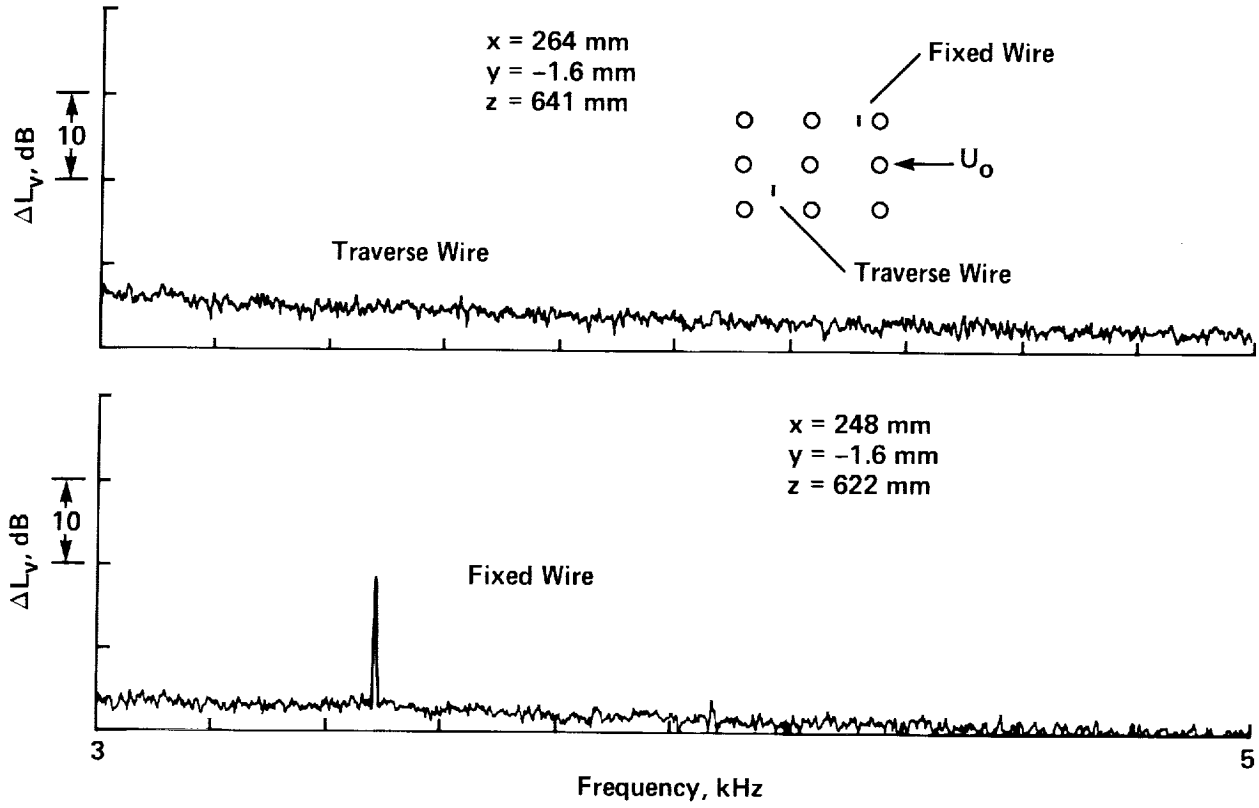

Figure 11.– Spectra from traverse and fixed hot wire; both wires were 1.6 mm from screen no. 1. The fixed wire was downstream of a hole; the traverse wire was between orifice rows. U_o = 39 m/sec.

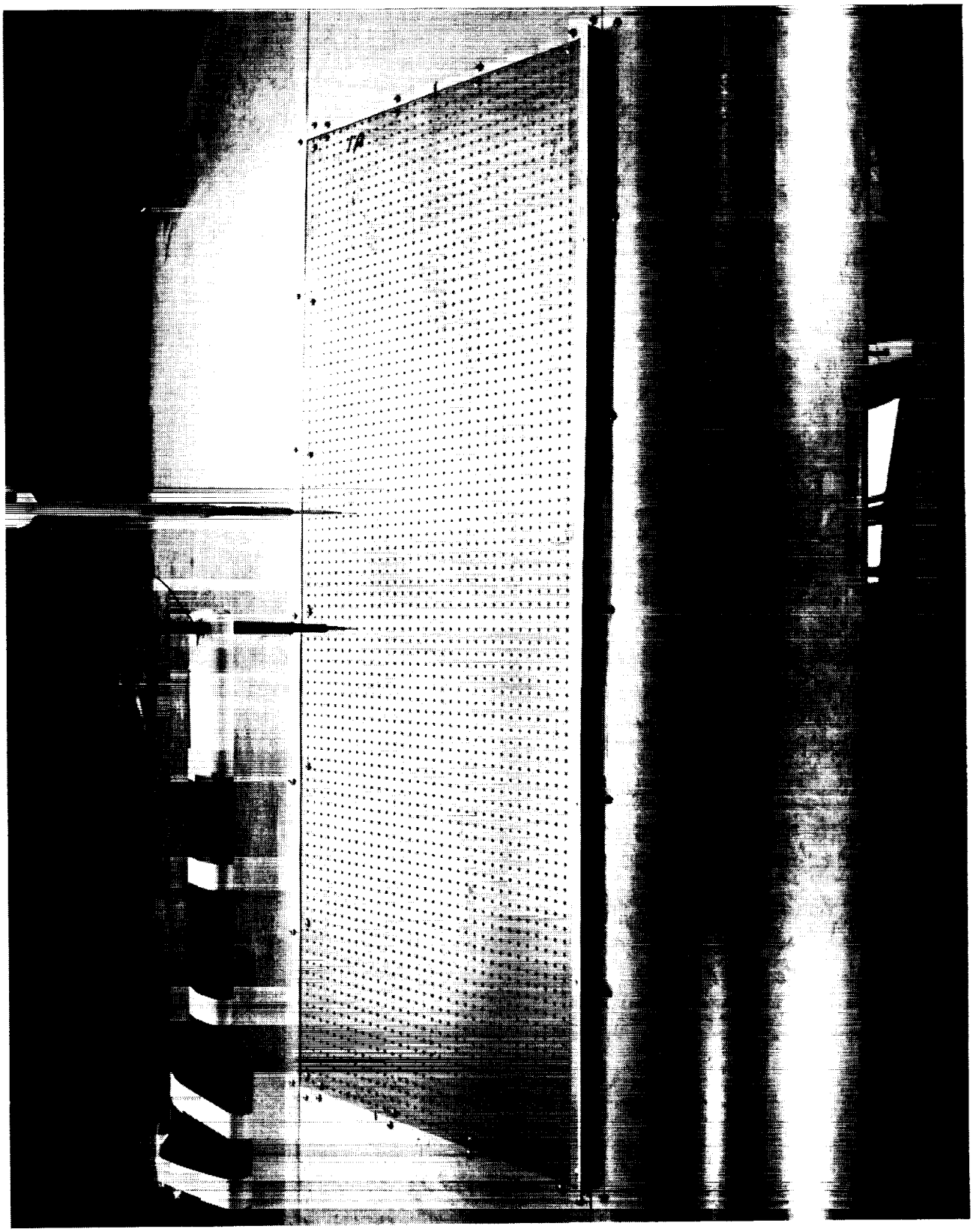

Figure 12.– A 17.5-mm angle (spoiler) attached to the leading edge of screen no. 1.

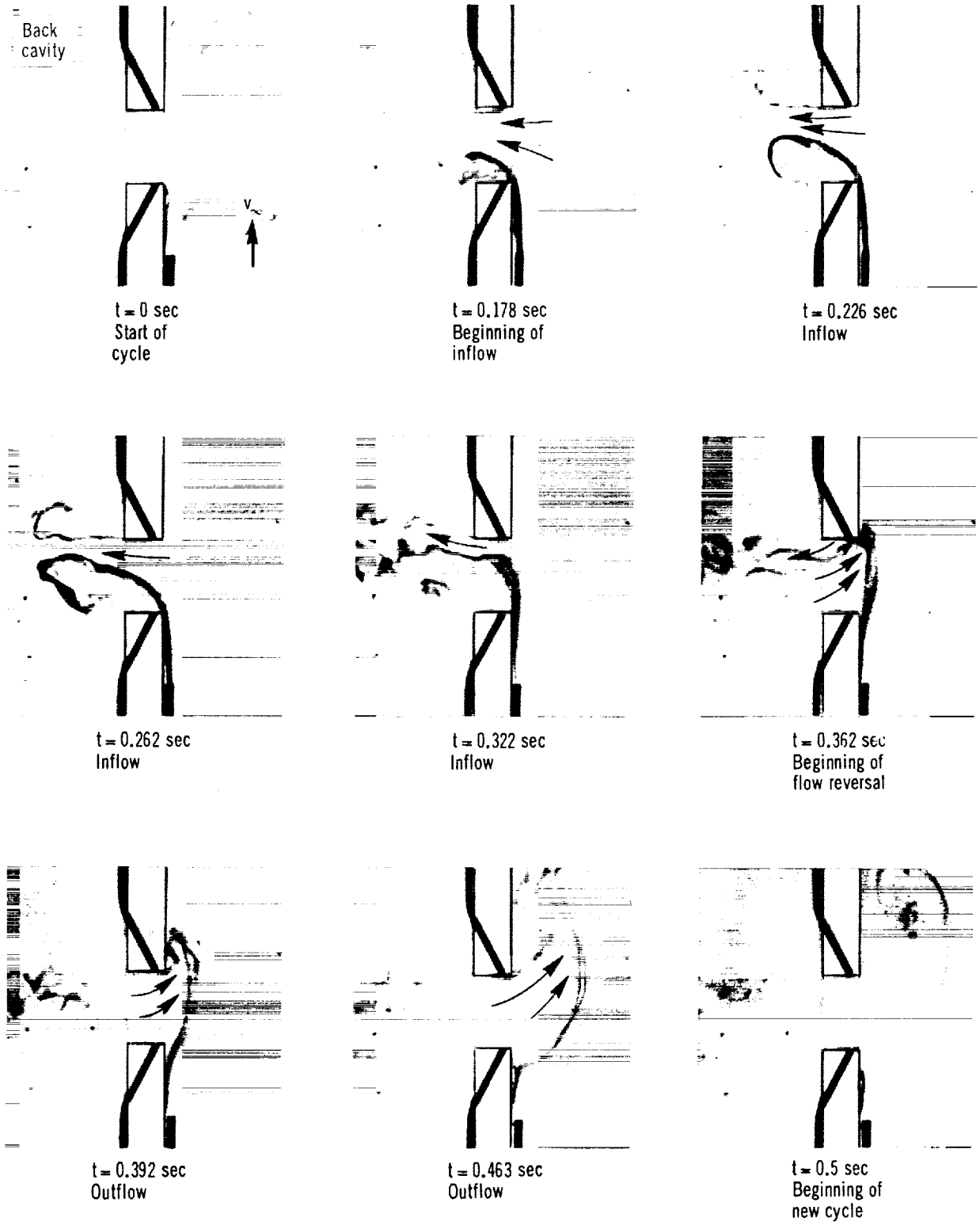

Figure 13.– Photographs of flow oscillations in the orifice of a Helmholtz resonator subject to 2 Hz simulated resonance and 0.3 m/sec grazing flow (from Baumeister and Rice, 1975).

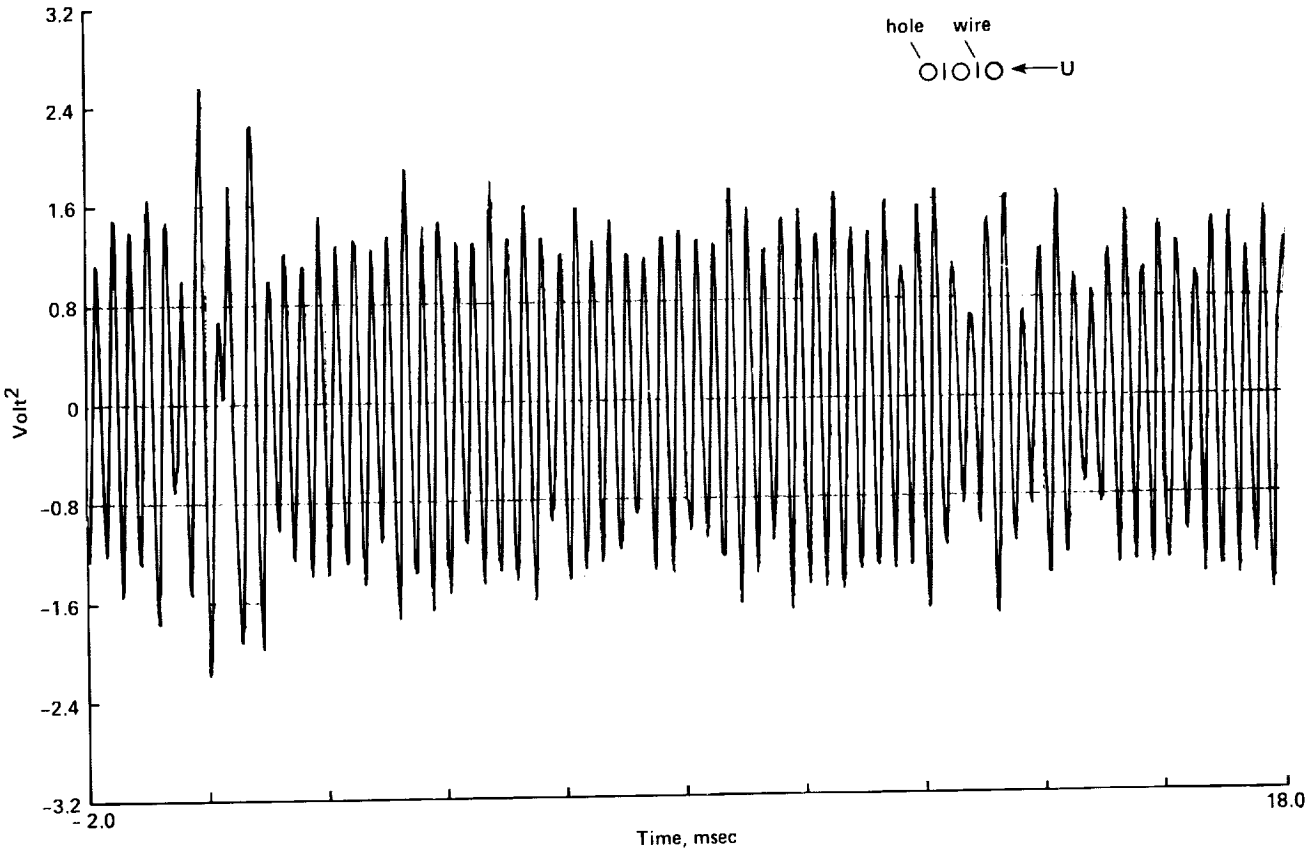

Figure 14.– Cross correlation of two hot-wire signals. Wires were separated streamwise 15.9 mm and were both 1.6 mm from screen no. 1. Periodic signal is from orifice vortex shedding. $U_0 = 41.5$ m/sec.

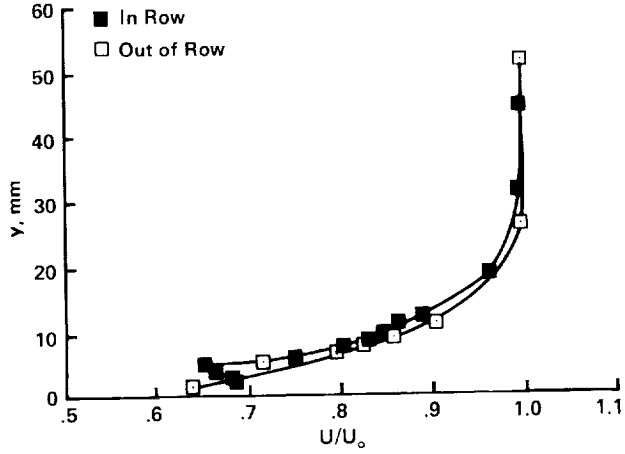

(a) In and out of an orifice row.

Figure 15.– Boundary-layer velocity profile measured on screen no. 1. $U_0 = 49$ m/sec.

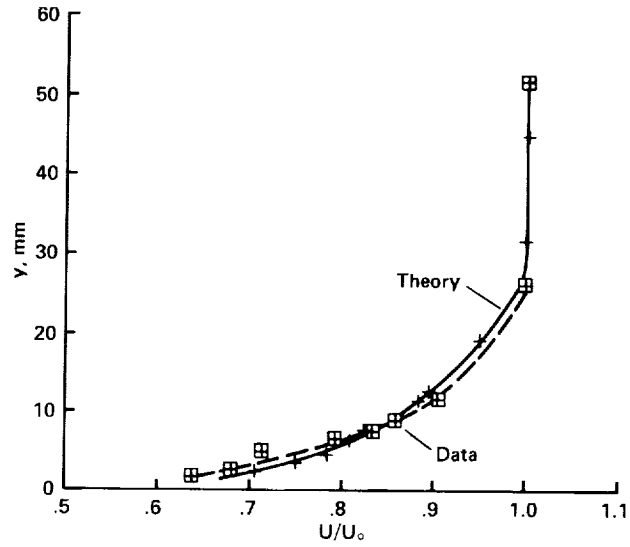

(b) Comparison of out-of-row data with a one-seventh power law curve for a turbulent boundary layer.

Figure 15.– Concluded.

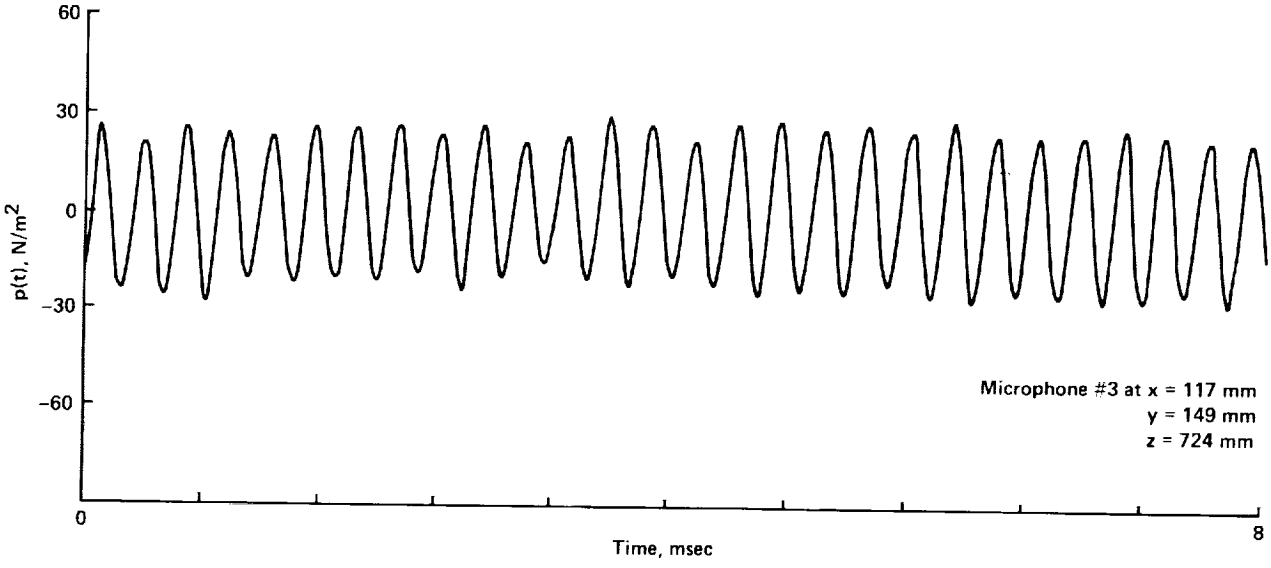

Figure 16.– Acoustic pressure time trace measured in the 302-mm-deep cavity with screen no. 1 installed. $U_0 = 41$ m/sec.

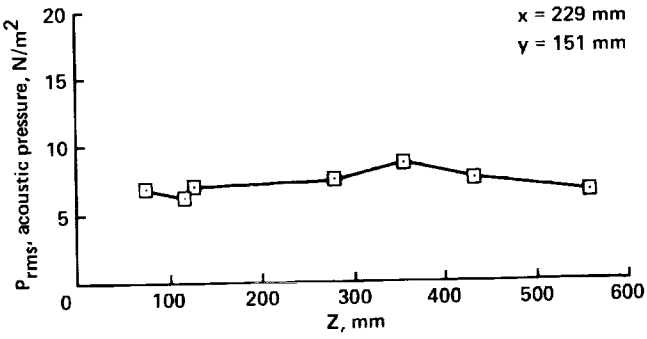

(a) Vertical survey.

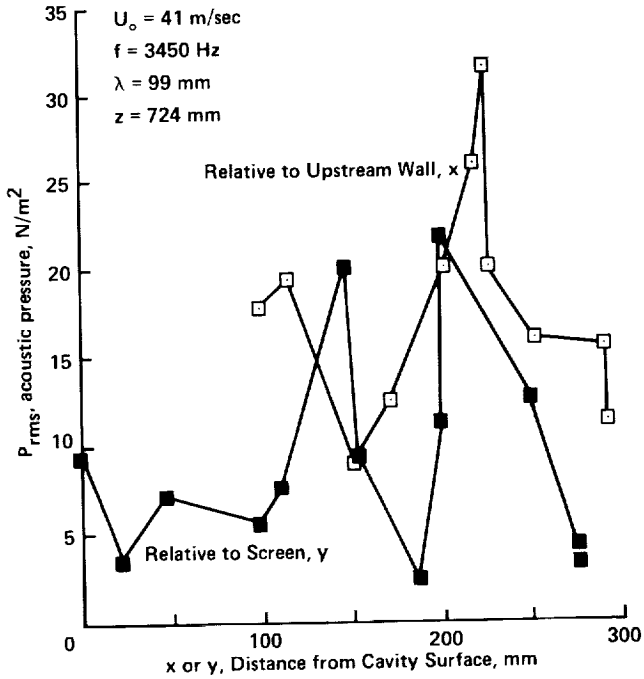

(b) Horizontal surveys.

Figure 17.– Variation of resonance acoustic tone amplitude with location in the 302-mm-deep cavity; screen no. 1. The frequency is 1825 Hz. U_o = 24 m/sec

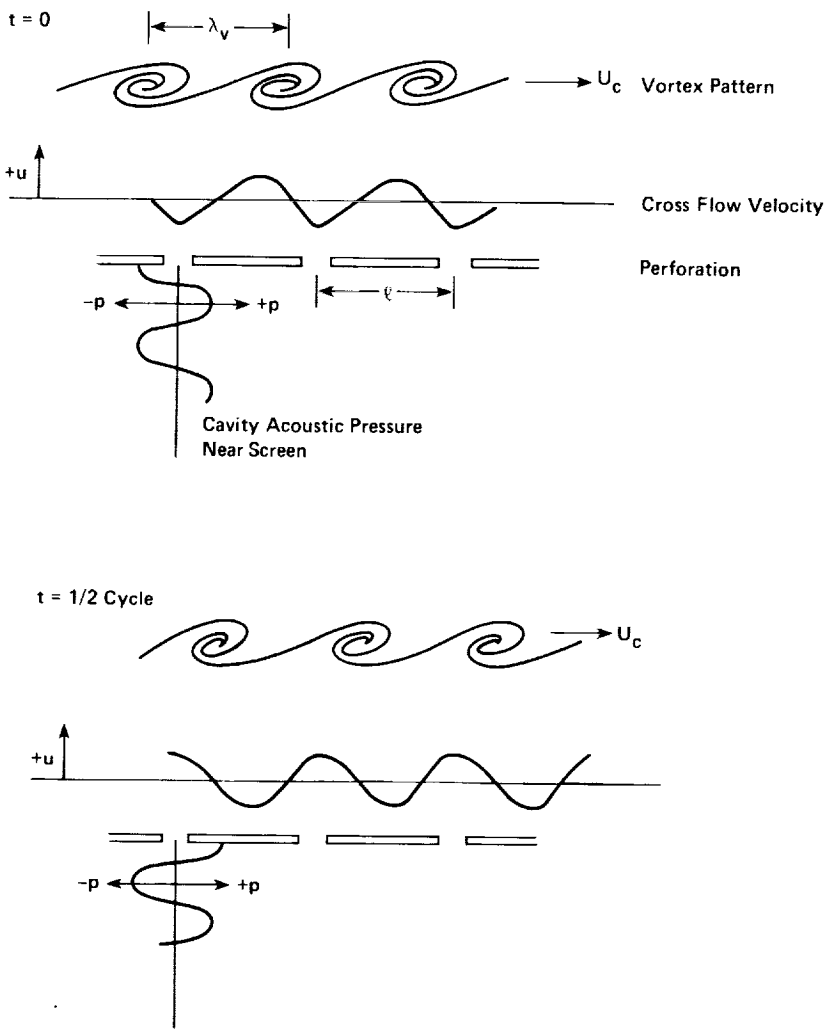

Figure 18.– Relationship among vortex street position, induced vortex velocity normal to the screen, and cavity pressures during resonance. $\frac{\lambda_v}{\ell} = 1.0$.

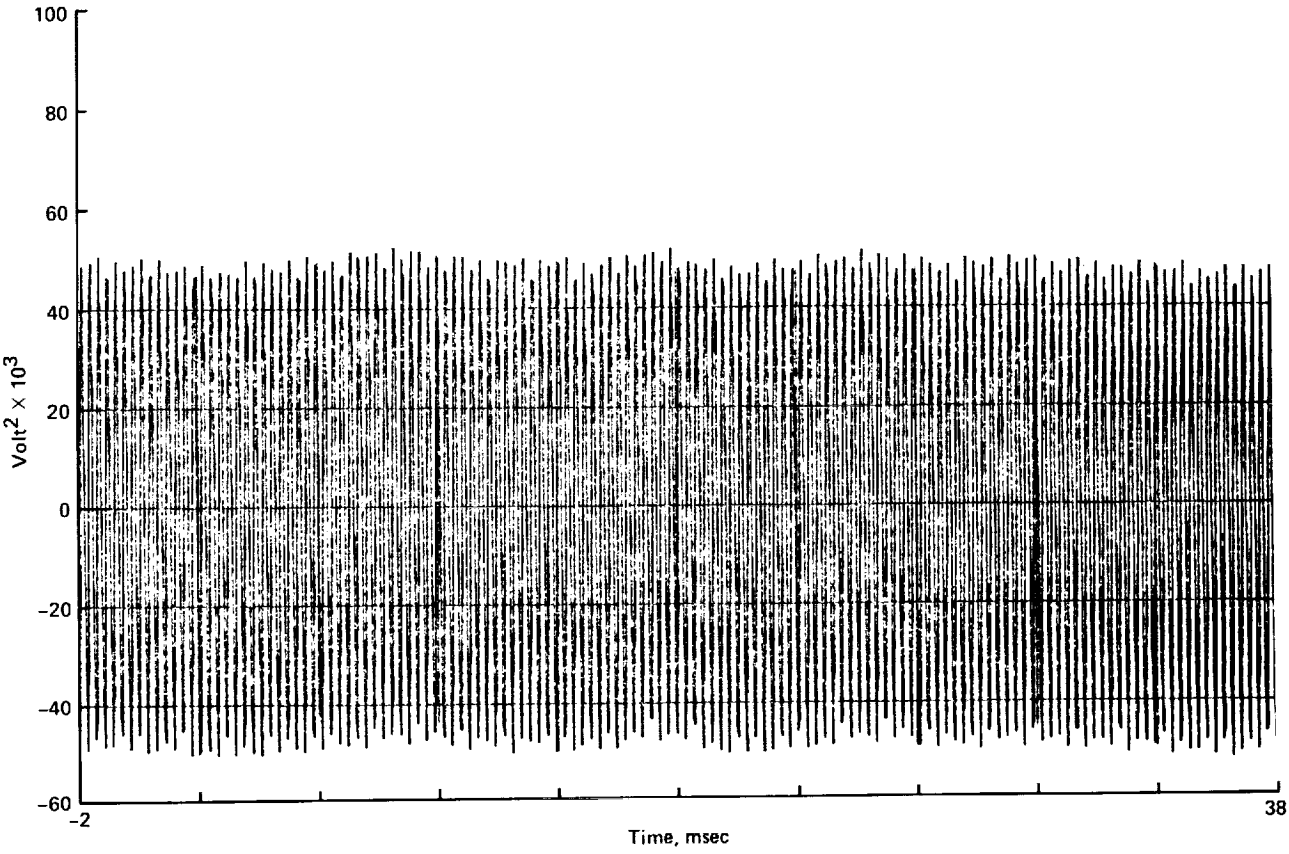

Figure 19.– Cross correlation of cavity microphone no. 3 and hot wire 1.6 mm from screen no. 1. U_O = 43.4 m/sec.

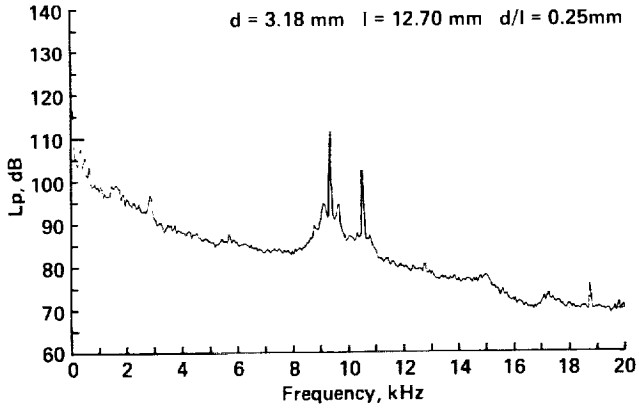

Figure 20.– Acoustic spectrum at microphone no. 2 with screen no. 1 over the 152-mm-deep cavity in the left vane (right vane removed). U_O = 92 m/sec.

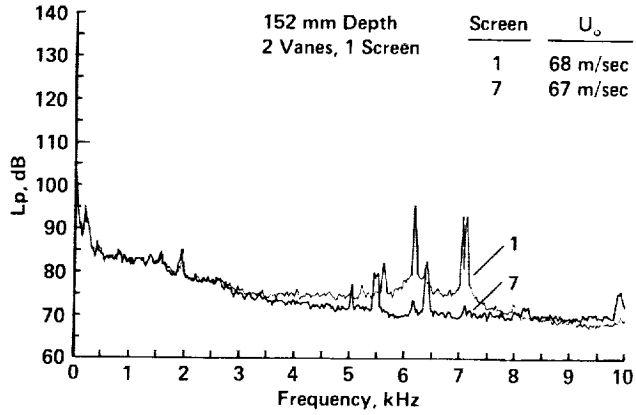

(a) ℓ = 4.37 mm hole spacing (screen no. 7).

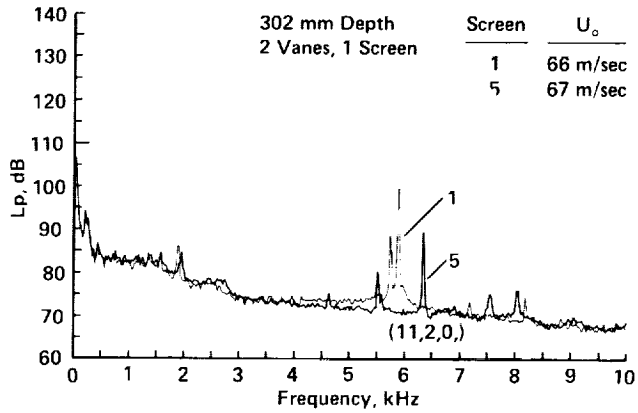

(c) ℓ = 6.35 mm hole spacing (screen no. 5).

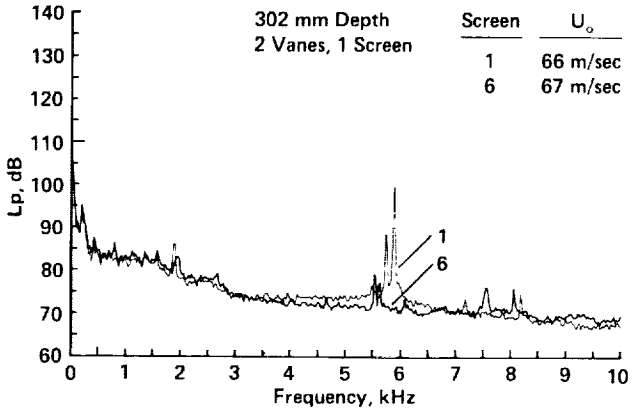

(b) ℓ = 5.16 mm hole spacing (screen no. 6).

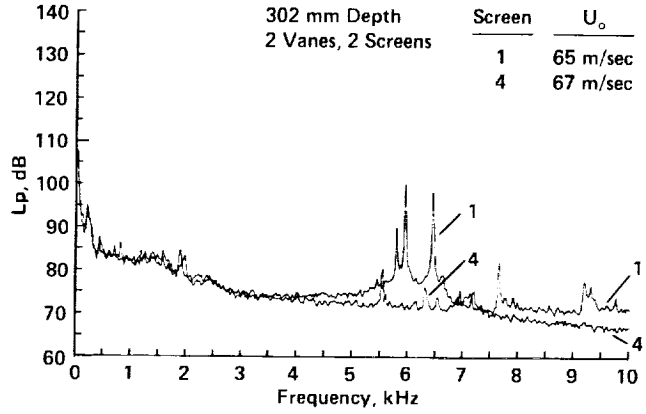

(d) ℓ = 8.73 mm hole spacing (screen no. 4).

Figure 21.– Acoustic spectra from cavity screens with 1.59-mm-diameter holes. Data from screen no. 1 with 3.18 mm diameter holes are plotted for comparison. Microphone no. 1. U_0 = 67 m/sec.

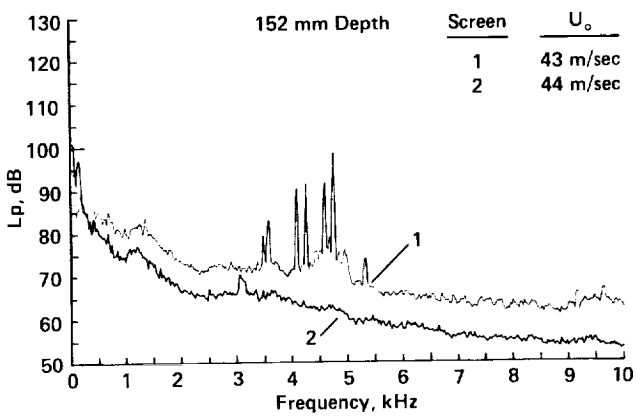

(a) $U_0 = 43$ m/sec.

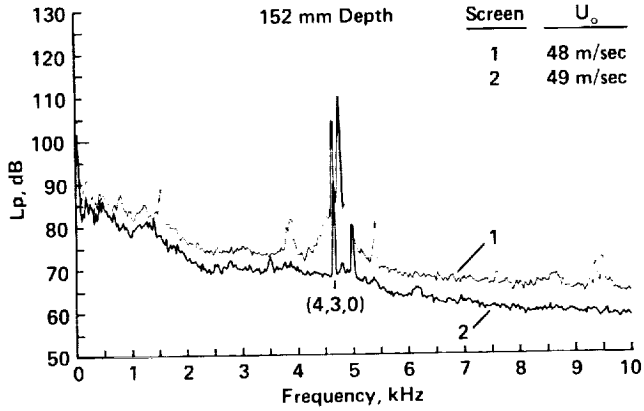

(b) $U_0 = 48$ m/sec.

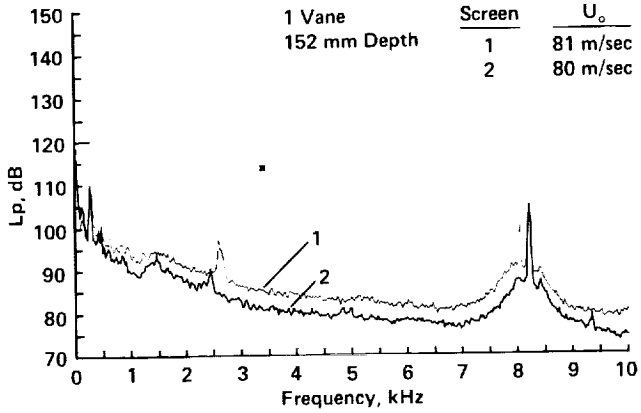

(c) $U_0 = 80$ m/sec.

Figure 22.– Acoustic spectra from screens no. 1 and no. 2 with 3.18-mm-diameter holes at three airspeeds. The hole spacings were 12.7 and 9.53 mm for screens no. 1 and no. 2, respectively. Microphone no. 2.

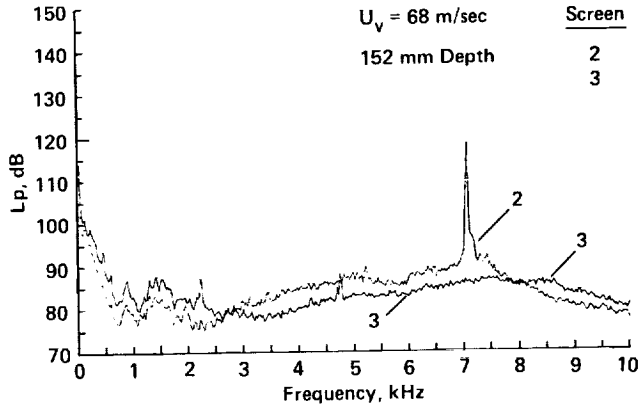

Figure 23.– Acoustic spectra from cavity screens no. 2 and no. 3 with 3.18-mm-diameter holes. Hole spacings were 9.53 and 6.35 mm for screens no. 2 and no. 3, respectively. $U_0 = 68$ m/sec. Microphone no. 3.

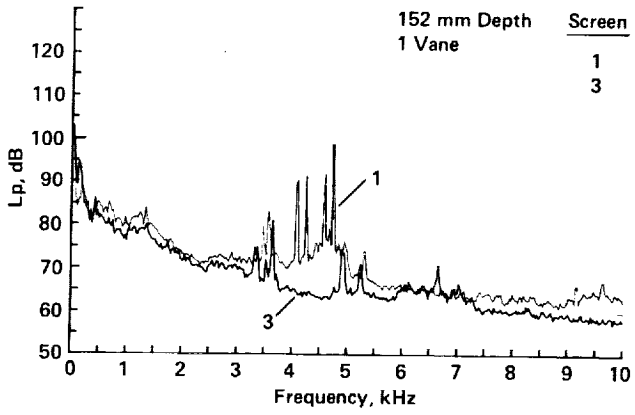

(a) U_0 = 43 m/sec.

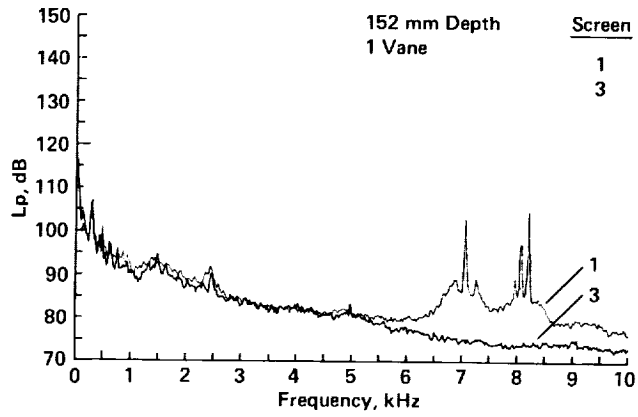

(b) U_0 = 75 m/sec.

Figure 24.– Acoustic spectra from cavity screen no. 3 with 6.35-mm-diameter holes. Data from screen no. 1 with 3.18 mm diameter holes are plotted for comparison. Microphone no. 2.

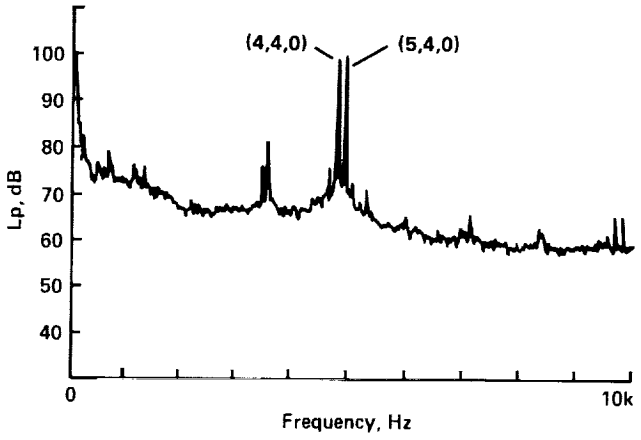

(a) U_0 = 48 m/sec.

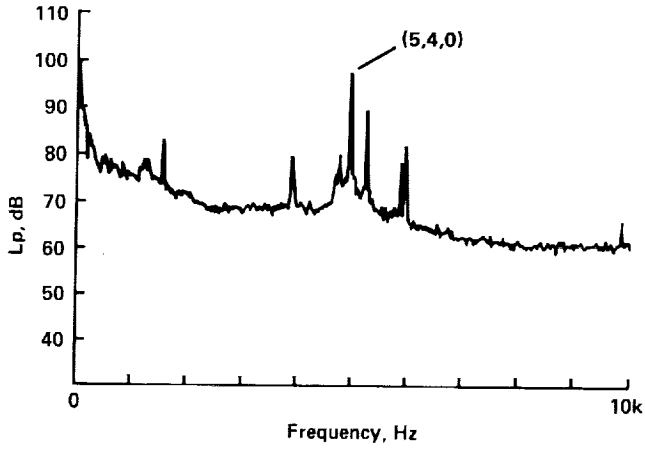

(b) U_0 = 54 m/sec.

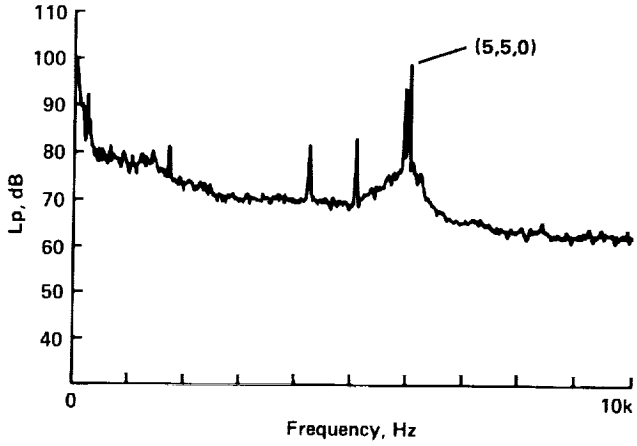

(c) U_0 = 59 m/sec.

Figure 25.– Acoustic spectra variation with airspeed; screen no. 1 over 152-mm-deep cavity; two vanes installed, right cavity sealed; microphone no. 1.

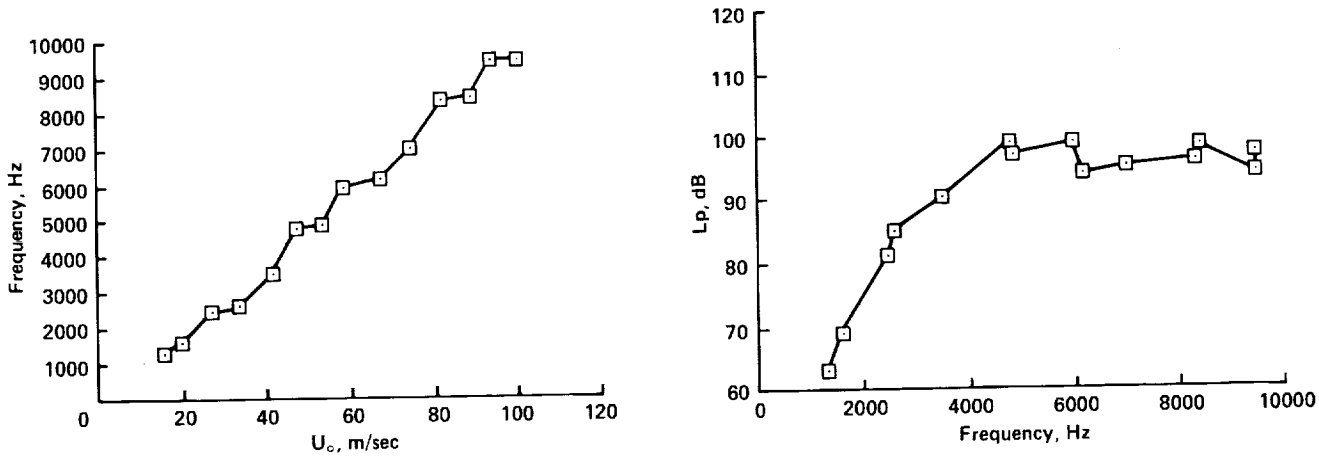

(a) Frequency variation.

(b) Amplitude variation.

Figure 26.– Variation of resonance frequency and amplitude with aispeed; screen no. 1 over 152-mm-deep cavity; two vanes, right cavity sealed, microphone no. 1.

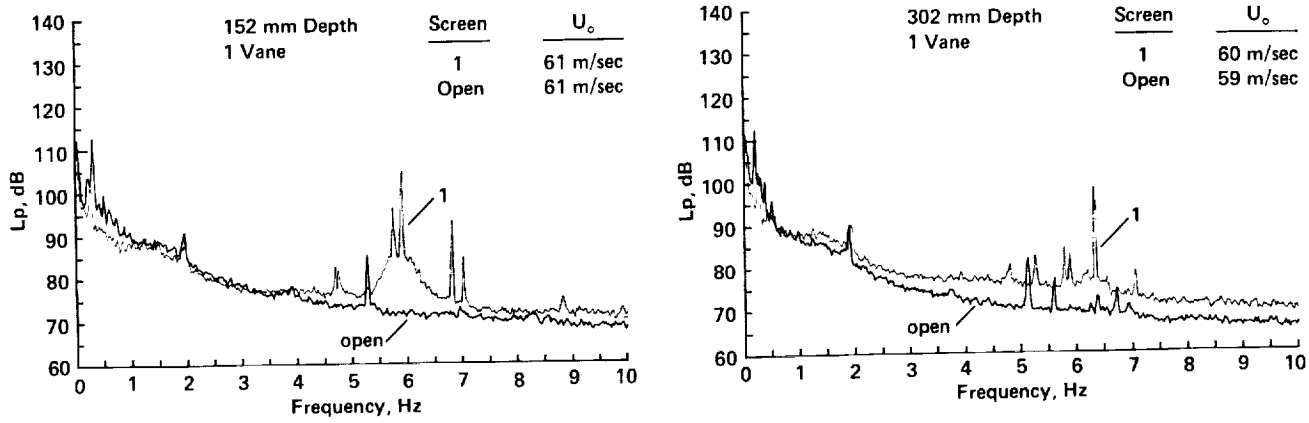

(a) 152-mm-deep cavities.

(b) 302 mm deep cavities.

Figure 27.– Comparison of acoustic spectra generated by screened and open cavities; microphone no. 2.

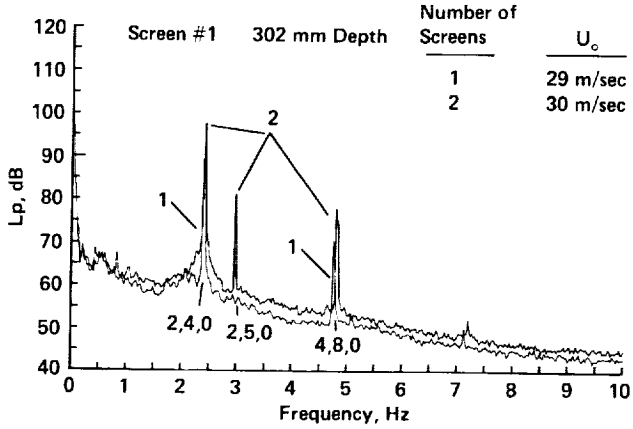

Figure 28.– Acoustic spectra from one cavity and from two cavities. Both vanes installed. Microphone no. 1. $U_O = 40$ m/sec.

NASA
National Aeronautics and Space Administration

Report Documentation Page

1. Report No.	2. Government Accession No.	3. Recipient's Catalog No.
NASA TP-3052		

4. Title and Subtitle	5. Report Date
Flow-Induced Resonance of Screen-Covered Cavities	October 1990
	6. Performing Organization Code

7. Author(s)	8. Performing Organization Report No.
Paul T. Soderman	A-89252
	10. Work Unit No. 505-61-11

9. Performing Organization Name and Address	11. Contract or Grant No.
Ames Research Center Moffett Field, CA 94035-1000	

12. Sponsoring Agency Name and Address	13. Type of Report and Period Covered
National Aeronautics and Space Administration Washington, DC 20546-0001	Technical Paper
	14. Sponsoring Agency Code

15. Supplementary Notes

Point of Contact: Paul Soderman, Ames Research Center, MS 247-2, Moffett Field, CA 94035-1000
(415) 604-6675 or FTS 464-6675

16. Abstract

This report describes an experimental study of screen-covered cavities exposed to airflow tangent to the screen. In this study, the term "screen" refers to a thin metal plate perforated with a repetitive pattern of round holes. Cavities are a necessary feature of many fluid systems, but the associated pressure fluctuations in cavities, both aerodynamic and acoustic, are often highly undesirable. In many cases, screen coverings are compatible with the intended communication between the cavity and airstream, but their interaction with the free stream can induce cavity acoustic resonance. The purpose of this investigation was to find the detailed aerodynamic and acoustic mechanisms responsible for screen-covered cavity resonance and to find ways to control the pressure oscillations.

Results of the study indicate that strong cavity acoustic resonances are created by screen orifices that shed vortices which couple with cavity pressure oscillations. The screen geometry plays a dominant role in the resonance. A method was found to avoid cavity resonance by choosing hole spacings such that shed vortices do not arrive at a downstream orifice in synchronization with cavity pressure oscillations. The proper hole pattern is effective at all airspeeds. It was also discovered that a reduction of orifice size tended to weaken the screen/cavity interaction regardless of hole pattern, probably because of viscous flow losses at the orifices.

The screened cavities that resonated did so at much higher frequencies than the equivalent open cavity. The classical large eddy rotation in the open cavity is replaced by a cavity acoustic resonance, which is triggered by orifice vortex shedding. Since that phenomenon occurs at the relatively small scale of the orifices, the excitation is typically of high frequency.

The wind tunnel study was made at airspeeds from 0 to 100 m/sec. The 457-mm-long by 1.09-m-high rectangular cavities had length-to-depth ratios greater than one, which is indicative of shallow cavities. The cavity screens were perforated in straight rows and columns with hole diameters ranging from 1.59 to 6.35 mm and with porosities from 2.6 to 19.6%.

17. Key Words (Suggested by Author(s))	18. Distribution Statement
Cavity resonance, Cavity pressure oscillations, Flow-induced resonance, Orifice flow oscillations, Aeroacoustics, Vortex shedding, Cavity screens	Unclassified-Unlimited Subject Category - 34

19. Security Classif. (of this report)	20. Security Classif. (of this page)	21. No. of Pages	22. Price
Unclassified	Unclassified	45	A03

NASA FORM 1626 OCT 86

For sale by the National Technical Information Service, Springfield, Virginia 22161

NASA-Langley, 1990